LBL-10994

Lawrence Berkeley Laboratory
UNIVERSITY OF CALIFORNIA

Materials & Molecular
Research Division

SLIDING WEAR, TOUGHNESS AND MICROSTRUCTURAL RELATIONSHIPS IN HIGH STRENGTH Fe/Cr/C EXPERIMENTAL STEELS

William J. Salesky
(M.S. thesis)

June 1980

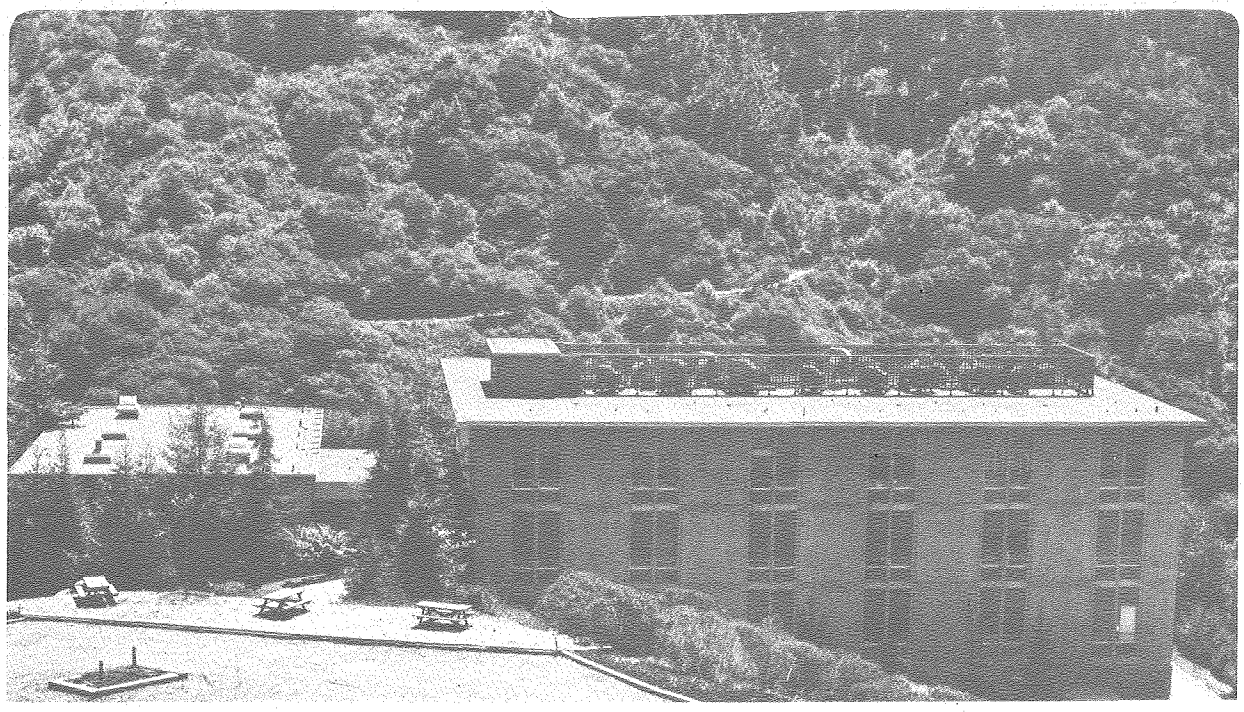

Prepared for the U.S. Department of Energy under Contract W-7405-ENG-48

DISCLAIMER

SLIDING WEAR, TOUGHNESS, AND MICROSTRUCTURAL RELATIONSHIPS IN HIGH STRENGTH Fe/Cr/C EXPERIMENTAL STEELS

TABLE OF CONTENTS

SLIDING WEAR, TOUGHNESS AND MICROSTRUCTURAL RELATIONSHIPS IN HIGH STRENGTH Fe/Cr/C EXPERIMENTAL STEELS

by

William J. Salesky

Materials and Molecular Research Division

Lawrence Berkeley Laboratory

University of California

and

Materials Science and Mineral Engineering Department

University of California

Berkeley, California 94720

ABSTRACT

Traditionally, hardness has been believed to be the major parameter influencing wear resistance of materials. Recently, it has been suggested that combinations of high strength and toughness may lead to optimum wear resistance. It is well-known that the martensite transformation can be exploited to provide a variety of strength-toughness combinations. Small additions of Mn or Ni to the Fe/4Cr/.3C martensitic alloys have been previously[42] shown to increase toughness while maintaining strength via increasing the volume fraction of retained austenite. The purpose of this study is to investigate the relationships between microstructure,

toughness, and sliding wear resistance for these experimental alloys. Comparative studies were also performed on several industrial alloys to provide a practical basis for comparison of these medium carbon experimental steels.

Wear tests were performed in the laboratory using a pin-on-disk machine. Small loads and low sliding speeds were employed to create a mild sliding wear condition. The surfaces of all worn specimens were examined by SEM to record surface characteristics. Conventional TEM techniques were used to determine the microstructures of the alloys prior to the wear testing.

The results of the study showed that the microduplex Fe/4Cr/.3C/2MN had superior wear characteristics over the commercial alloys examined. A correlation was obtained between wear resistance and percent retained austenite, which in turn is related to the Charpy impact energy. However, wear resistance was observed to be independent of hardness for the Fe/Cr/C alloys.

Although the microstructural mechanism by which sliding wear occurs was not determined, plastic flow across the worn surface coupled with delamination events appears to be the cause of wear. The results indicate the possible significance of crack initiation as a primary factor in this mechanism.

I. Introduction

A. Background

A large percentage of the operating costs for heavy industries such as earth moving, mining, and mineral processing are due to metal wear. In the United States and Canada alone, more than a billion pounds of steel are consumed each year in mining and mineral processing operations.[1] This amounts to more than 1% of the total quantity of steel produced in the United States and Canada being consumed by wear. Although the implicitly enormous replacement costs have motivated extensive engineering wear-related research to generate vast amounts of empirical data, there is currently little, if any, fundamental understanding of the relationship between microstructure, mechanical properties, and wear. The difficulties in establishing such a relationship stem from the complex nature of most wear systems and the difficulties in measuring, adjusting, and controlling relevant material parameters which influence wear.[2]

Although a majority of wear problems arising in earth moving, mining, and mineral processing involve three-body abrasion, sliding wear was chosen for this study. The reason for this is that sliding wear tests are easier to perform than abrasive wear tests. Consequently, consistent trends of wear behavior could more easily be established for studying the effect of microstructural variations on a (surface deformation) wear process. Sliding wear itself involves two mating surfaces, subjected to a load perpendicular to their contact plane, one moving relative to the other. The absence of an abrasive medium

is the main difference between sliding wear and three-body abrasion. Consequently, sliding wear, which is the loss of material from a surface, occurs by surface-subsurface deformation processes. However, the specific microstructural mechanisms by which sliding wear occurs has been the focus of controversy for well over 25 years.[3-29]

Recently, the "Delamination Theory" has been suggested by Suh[25,26] in which sliding wear occurs by subsurface deformation, crack nucleation and crack propagation. Although there has been some disagreement about the specific dislocation mechanics involved[18-21] and the limits of applicability, this theory gives a more tangible account for the evolution of plate-like wear debris normally observed in sliding wear than those previously proposed.[3-24] Consistent with other investigations,[19, 20, 30-32] Suh concluded that in most situations optimum wear resistance is achieved through design of microstructures which exhibit high toughness-strength combinations. By Suh's theory, high hardness is necessary to resist crack initiation and high toughness to resist crack propagation. Unfortunately, in most engineering materials, high strength is achieved at the expense of toughness and vice versa. However, specialized microstructures such as composites or duplex structures have shown promise for achieving increased high strength-toughness combinations.[33,41,50] It is, therefore, the objective of this investigation to examine the wear behavior of one such type, namely, an austenite-martensite microduplex structure.

B. Choice of Alloy Systems

It is well known that the martensitic transformation can be exploited to produce a variety of toughness strength combinations in high strength steels. While the most effective method for increasing the strength of martensitic steels is to increase the carbon content, their toughness deteriorates monotonically.[33] Consequently, over the past several years at Berkeley, a systematic study of the influence of alloying elements and heat treatments on martensitic microstructures and resultant mechanical properties, especially toughness, has been performed on a series of ternary Fe/Cr/C and quaternary Fe/Cr/C/Mn (or Ni) alloys.[33-50]

The result has been the development of steels of superior strength and toughness combinations through control of the duplex martensite-austenite microstructure. Because of their high toughness:strength ratio, it is apparent that these martensitic steels may be useful for wear-resistant applications. It is the purpose of this study to initiate a systematic program to assess and improve the wear behavior of the Fe/Cr/C/Mn alloys and attempt to relate wear behavior to microstructural features.

The microstructures of these Fe/Cr/C alloys are basically dislocated lath martensites surrounded by continuous thin films of stable retained austenite as schematically shown in Fig. 2 and imaged in Fig. 7. It has been shown previously that increasing the Mn content up to 2 wt.% serves to increase the volume fraction of retained austenite up to 6% via lateral film thickening with little or no change

in the martensite substructure.[42] Yet, the heat treatments applied to these alloys (Fig. 1) also affect the amount of retained austenite. The double heat treated, fine grained material had consistently greater amounts of retained austenite than that in the single heat treated coarse grained condition, regardless of Mn content.[42] An upper limit of 3% Mn has already been established as beyond this level undesirable twinned martensites are observed.[35]

The significance of the increasing austenite content via alloying and heat treatment stems from the observed[42,43] increases in Charpy V-notch impact energy and plane strain fracture toughness (K_{IC}) with austenite content (Table 2). This trend of increasing toughness properties with austenite content was realized at approximately constant strength hardness levels (i.e., 45-50 R_c). In these materials it is then possible to study the effect of toughness or wear behavior while maintaining constant hardness strength levels. Therefore, wear measurements were made on several Fe/Cr/C/Mn (or Ni) alloys in the quenched and tempered conditions. In some specimens, temper martensite embrittlement was induced to compare "tough" to "brittle" conditions for the same alloy composition.

Since no ASTM standards have been set for sliding wear measurements the pin-on-disk configuration was chosen since it is simple, well known[22,25,51] and a reproducible wear test. Trends of wear behavior were then established and contrasted with microstructure and mechanical properties. A parallel wear program was conducted on several "equivalent" commercial wear resistant mild steels to provide

a basis for comparison for the experimental alloys. Transmission electron microscopy was performed on the commercial materials to investigate their microstructures. Mössbauer spectroscopy was done on all the materials to quantitatively determine the amount of retained austenite present in the microstructure. Scanning electron microscopy was also done on all worn surfaces to attempt to elucidate the mode by which wear occurs.

II. Experimental Procedure

A. Materials

1. Preparation

The experimental Fe/4Cr/.3C/0-2Mn and Fe/4Cr/.3C/5Ni alloys used in this investigation were from the same heat of material used in previous studies.[42,43] These materials were vacuum induction melted by Daido Steel Corporation in Japan to the chemistries shown in Table 1. The as-received 2.5" wide by 1" thick bars were subsequently homogenized in an argon atmosphere at 1200°C for 24 hours, followed by furnace cooling. Commercial materials were selected to provide a basis for comparison. These materials are high strength steels with approximately the same strength levels as the experimental alloys.

The commercial alloys shown in Table 1 were used in the as-received condition. Abrasaloy was developed by Atlantic Steel Corporation, New York City, New York. Astralloy was prepared by Astralloy-Vulcan Corporation, Birmingham, Alabama. Firmex was designed by International Alloy, Cleveland, Ohio. AISI 4340 was purchased in the vacuum-melted condition and subsequently quenched and tempered.

2. Heat Treatment

Heat treatments (Fig. 1) were performed on the experimental alloys so as to produce a microstructure of dislocated lath martensite with continuous interlath film of retained austenite (Figs. 2,6). A single and double heat treatment cycle (see Fig. 1) was performed to produce approximate prior austenite grain sizes in Mn alloys of 300μm and 30μm, respectively, while in the Ni alloys, 160μm and 30μm, respectively. Austenitizing heat treatments were performed for one hour per inch of

specimen thickness in a vertical tube furnace, with temperature control of ±5°C, under a flowing argon atmosphere followed by an agitated oil quench. Although some specimens were treated in the as-quenched condition, tempering was performed on others for 1 hour per inch of specimen thickness in a salt pot followed by a water quench.

Most of the commercial alloys were received in the quenched and tempered condition, consequently no heat treatment was necessary. AISI 4340 was austenitized at 1100°C under conditions identical to the experimental materials.

B. Microstructure

1. Optical Metallography

Optical metallography was performed on the commercial materials to determine the microstructural character and to record any bulk phenomena observed. Specimens were cut from heat treated material, mounted in cold mount, abraded on silicon carbide papers down to 600 grit, and diamond polished with 1 micron paste on microcloth. The microstructure was revealed via 2% Nital etching.

2. Transmission electron microscopy (TEM) was performed only on the commercial materials, since in previous studies[42-45,48] detailed electron metallography had already been done on the experimental alloys. Thin foils for TEM were obtained by cutting 20 mil (500μm) slices from the heat treated steel via slow feed, flood cooled, diamet saw. These slices were chemically thinned to approximately 5 mils (130μm) in a 4% solution of HF in H_2O_2. The resulting thin slices were spark cut into 3.0mm disks which were abraded down to 600 grit paper to a thickness of 1-2 mils

(25-50μm). Final polishing was done in a twin-jet electro-polishing apparatus with a room temperature electrolytic solution of 75 gm. CrO_3, 400 ml CH_3COOH, and 21 ml distilled water until there was a hole at the disk's center. Polishing voltage was 30 to 40 volts at 32 to 38 milliamps. The thin foils were examined in a JEOL JEM 7A and Philips EM301 microscopes operated at 100kV.

3. Mössbauer Spectroscopy

Mössbauer spectroscopy was performed on excess heat treated experimental and commercial material to quantitatvively determine the average volume fraction of retained austenite present in the respective microstructures. Although it would have been desirable to also perform Mössbauer analyses on the surface of the worn specimens, the worn areas were too small (approximately 1400μm in diameter) to obtain an accurate analysis. Mössbauer spectroscopy was compared to prior X-ray analysis because of the facility provided by the Mössbauer technique for qualitatively determining small (∿5%) volume fractions of retained austenite due to the absence of texture effects, particularly in localized regions.[52] The prior X-ray data were those of Rao and Thomas[53] using the method[54] of R.L. Miller at U.S. Steel.

C. Wear

1. Specimen Preparation

The majority of the experimental steel wear specimens were machined from the undeformed regions of heat treated compact tension specimens used in a previous study[42] to obtain K_{IC} information. The specimen blank shown in Fig. 3 was cut from the bulk and sectioned as shown on a flood-cooled, slow feed, silicon carbide diamet saw. The

resulting bars were turned down on a lathe to form 1/4" diameter hemispherically tipped cylindrical pins. Five to ten mils were removed from the surface of the hemisphere by light grinding under flood cooling on a Norton surface grinder with 400 grit diamond wheel to remove micro-structural damage induced by turning.

It was observed that scatter in the data could be reduced by polishing the surfaces of the specimens after final grinding. Consequently, the hemispherical surfaces on all wear specimens were polished to remove grinding scratch using Buehler 600 grit abrasive paper followed by 1 micron diamond paste on microcloth while the specimen was rotating in a lathe at 500 rpm. Care was also taken during polishing to apply light loads so as to minimize specimen heating. Scanning electron microscopy at 5000 to 10,000X showed that few scratches remained on the hemispherical surfaces after polishing.

The specimens were hand cleaned in N-heptane to remove oil and dirt accumulated during preparation. Ultrasonic cleaning for a minimum of 5 minutes in acetone followed by alcohol was done to remove residual impurities left by the solvents. The specimens were then placed in a vacuum dessicator for a minimum of 20 minutes to insure removal of moisture left by the alcohol.

The specimen weight was measured prior to testing on a Mettler H54AR analytical balance to an accuracy of $\pm$.01 mg. Each specimen was weighed three times and the median reading recorded. After wear testing, the specimens were recleaned in acetone and alcohol and then re-weighed. The measured weight loss of the pin was determined and was used to compute wear resistance as shown below:

$$\text{Wear Resistance} = \frac{1}{\text{Wear Rate}}$$

$$= \frac{\text{Sliding Distance}}{\text{Volume of Metal Removed}}$$

$$= \frac{(\text{Material Density})(\text{Sliding Distance})}{(\text{Weight Loss})} \ \text{mm/mm}^3$$

2. Wear Measurements

Wear testing was done utilizing a pin-on-disk wear machine fabricated at Lawrence Berkeley Laboratory in 1977 (see Figs. 4,5). Since no ASTM standard has been set for any sliding wear measurements, the test parameters used here were selected to produce a measureable amount of mild sliding wear in the absence of specimen heating. Consequently, the pins were worn for 4 hours each at 10 rpm disk speed under 1 kg deadweight load. The disk against which the specimens were worn was .95 cm thick, 12.7 cm in diameter, AISI 4340 which was quenched and tempered to $53R_C$. Each test was conducted on a fresh wear track at constant radius of 4.92 cm. Hence, only one wear test was performed on each side of the disk. The disk was then ground to remove 6 mils (150μm) from each side and subsequent tests were then performed. Only one wear disk was used for this study to insure reproducibility. Periodically, the hardness of the disk was checked and was found not to change. The surface of the wear track was also periodically examined and no metal transfer appeared to occur between the pins and the disk.

A minimum of 3 specimens was used to establish each datum point for all the steels tested. It should be noted that friction forces were also recorded for completeness as shown in Tables 2 and 3 via resistive strain gauges (shown in Fig. 5) from which the output was amplified by a Dynamic

DC amplifier and recorded on a Moseley 680 Strip Chart Recorder.

3. Fractography

Detailed scanning electron microscopic studies were performed on the worn surfaces of all specimens tested using and AMR 100 SEM equipped with an energy dispersive X-ray (EDX) analyzing apparatus.

III. Results and Analysis

A. Microstructure

1. Experimental Alloys

The microstructures of the experimental alloys have been well documented[42-45,48] and, in the quenched condition, are known to consist of dislocated lath martensite[55-70] with continuous interlath films of retained austenite (typically observed in Fig. 6). Upon tempering at 200°C, Widmanstatten cementite[70] precipitation occurs within the martensitic laths as seen in Fig. 7. Tempering at 300°C induces transformation of the retained austenite to interlath ferrite and cementite (Temper Martensite Embrittlement) to produce the structure seen in Fig. 8. The mechanical properties evolving from these microstructures are shown in Tables 2A and 2B.

Previous X-ray analyses[42] have shown an increase in the volume fraction retained austenite from approximately 0% to 2% with alloying of up to 2% Mn in the Fe/Cr/C system. In this study, Mössbauer spectroscopy, performed on the same heat of material used in previous studies[42,44] shows consistently higher percentages of retained austenite than determined by X-ray[54] (see Appendix I). Although one would not expect such a large difference, as shown in Fig. 9, between X-ray and Mössbauer techniques, it is well known that quantitative X-ray analysis is sensitive to crystal orientation. Within the prior austenite grain obviously a single variant of austenite exists. Therefore, depending on the prior austenite grain size, a monovariant is contributing to the X-ray diffraction.[42] This is similar to the situation wherein preferential crystal orientation exists, such as can be produced by rolling, which acts to reduce the intensities of certain

austenite peaks. Consequently, this fact and the small volume fractions of retained austenite present in these alloys complicates the analysis.[46] Mössbauer, however, is insensitive to crystal orientation. Thus, one would expect higher austenite volume fraction values from the Mössbauer than the X-ray technique. However, the absolute magnitude of these numbers is not of the greatest significance, but the fact that both techniques show the same trend of increasing retained austenite with Mn addition is important.

2. Commerical Alloys

Due to the proprietary nature of Abrasaloy, Astralloy, and Firmex, little information was available regarding their microstructure. Optical metallography and scanning electron microscopy (SEM) as shown in Figs. 10 and 11 suggested the microstructures were martensite and/or bainite. Inclusions elongated in the rolling direction were observed in Firmex (Fig. 11a). An SEM micrograph of the inclusions with corresponding X-ray map showed the inclusions to be rich in sulphur; thereby indicating that they are probably MnS rolling inclusions (Figs. 11b and 11c).

Transmission electron microscopy revealed the bainitic nature of the quenched and tempered Abrasaloy (Figs. 12 and 13). Interlath as well as intralath carbides, which are predominantly cementite, are easily resolved in the dark fields of micrographs of Figs. 12b and 13b. Mössbauer spectroscopy showed less than 0.3% of retained austenite to be present in the structure. The absence of retained austenite, the presence of cementite, and the low hardness ($34.5R_C$) suggests this material is bainitic.

Astralloy, however, appears to be a complex martensite (Fig. 14). No interlath carbides could be resolved, so the structure is not upper

bainitic. Mössbauer spectroscopy indicated greater than 20% paramagnetic phase was present. Attempts to detect via TEM retained austenite were unsuccessful. Due to the air-cooling from 850°C, the absence of interlath carbides and significant amounts of Cr and Ni in the alloy, the 20% or more paramagnetic phase is believed to reflect the presence of a large number of alloy carbides. A small volume fraction of microtwins was observed as shown in Fig. 15.

Firmex appeared to be a combination of bainite and martensite non-uniformly distributed (Figs. 16 and 17). Widmanstatten cementite was observed extensively throughout the bainitic regions. The variation of microstructure in this steel was striking. Mössbauer spectroscopy showed 1-1/2% of retained austenite to be present, however, attempts were not successful to image the austenite.

Since a large amount of work has been performed[55-58] on AISI 4340 and its structure is well-known to be martensitic, it was not examined under TEM in this study. Mössbauer spectroscopy showed 6% austenite for the AISI 4340 material. The microstructure of this alloy has been shown to be dislocated lath martensite with non-continuous interlath retained austenite. Although its structure is similar to the experimental materials, its toughness is substantially less (see Tables 2 and 3). In summary, microstructures of the commercial alloys are qualitatively similar to the experimental steels, but clearly have not been designed to the same scheme (Fig. 2) for good toughness.

B. Wear Measurements

Prior to the analyses and evaluation of any experimental wear data, some considerations of the limitations are essential. Since the wear form

and degree are the products of a tribological system[2,3,20,21,22,26] environment, testing machine design, loading, velocity, specimen geometry, as well as wear component material parameters directly affect the amount of wear observed. Due to the strong influence of testing geometry and loading conditions, numerical wear rate values generated in a modeled system often poorly correlate with that observed in an applied mechanical system. However, laboratory data are useful for establishing relative trends of behavior for comparative alloy evaluation. It is in this vein that the data contained herein will be discussed. Considerable effort was made to minimize the statistical scatter through careful experimental technique to enable subtle trends of wear behavior to also be observed.

A summary of mechanical properties, friction and wear data is shown in Tables 2 and 3. These results are from a 4-hour duration, 1 kg loaded, 10 rpm speed sliding wear test. These conditions appear to represent a steady state wear as observed for the double heat treated 2% alloy (Quatough) and a commercial alloy steel, Abrasaloy (see Fig. 18).

1. Experimental Alloys

The heat treatments performed on the experimental alloys appeared to have a profound effect on the sliding wear resistance. In all cases, the double heat treatment gave rise to 20 to 30% higher wear resistance than single heat treatment. Although prior austenite grain size is refined and retained austenite content increased by this double heat treatment, it is not clear which has a greater effect. However, Fig. 19 does show that a reduction in prior austenite grain size increases sliding wear resistance.

Increasing the Mn or Ni content of the Fe/Cr/C base alloy has been previously observed to increase the volume fraction of retained austenite with little or no change in the martensite substructure or bulk hardness.[42] It was previously suggested[40-43,46,47] that this austenite was responsible for the increased toughness of the higher Mn alloys. However, the mechanism (i.e. crack branching, crack blunting, "trip," etc.) by which austenite acts to increase toughness in this material is still not clearly known. From the present work there appears to be a trend of increasing wear resistance with austenite content. However, as shown in Fig. 20, this trend will probably reach a maximum in the present alloying system and decrease due to the onset of substructural twinning as observed[11] for the 5Ni alloy and known to occur for Mn alloys greater than 2.5%.[33]

Considering the effect of tempering on sliding wear resistance, the increase in wear resistance and toughness of the grain refined, 200°C tempered condition over the as quenched condition appears to be due to the lack of auto tempering[42] observed for the fine grained 2% Mn alloy. However, the drop in wear resistance for both the fine grained and coarse grained 2% Mn alloys after 300°C tempering appears to be due to the decomposition of retained austenite to form interlath cementite and carbide classically called temper martensite embrittlement. It should be noted that there is also a 50% reduction in impact toughness and a 10% reduction in hardness due to the onset of temper martensite embrittlement. However, in the 500°C tempered condition (temper embrittlement) there was little further degradation of sliding wear resistance even though impact toughness was observed to decrease slightly. Thus, from these results, it appears

that the presence or the lack thereof of the retained austenite has the most significant effect on wear.

Hardness has traditionally been believed to be the most significant factor affecting wear resistance. However, hardness is not a fundamental material property, but a reflection of tensile strength.[59] Consequently, materials with the same tensile strength but different yield strengths and different strain hardening behavior may reflect the same hardness values but are often observed to wear at different rates.[58] The results of the present study reinforce this point by showing a variety of wear resistances at constant hardness levels for the experimental Mn and Ni steels (see Fig. 22); whereas, the commercial materials exhibit a decreasing wear resistance with increasing hardness. This result appears to suggest that toughness and morphology play a significant role in determining sliding wear resistance.

Attempts to relate wear resistance with classical toughness measurements yielded a weak correlation between plane strain fracture toughness and sliding wear resistance (Fig. 23). However, an apparent trend of increasing wear resistance with Charpy impact energy was observed for the 2% Mn steels (Fig. 24), with an exception for the as-quenched condition. The significance of these results will be discussed later.

2. Commercial Alloys

Comparison of sliding wear results of commercial to experimental alloys indicate that the experimental steels are more sliding wear resistant (see Tables 2 and 3 and Fig. 25). However, the results for Abrasaloy are within the experimental scatter band of the double heat

treated 2% Mn alloy. Results for Firmex, Astralloy, and 4340 are considerably less favorable than that for Abrasaloy. The observed trend is surprising since Abrasaloy is the softest of the commercial steels (see Fig. 22). This result implies toughness and morphology as well as hardness are significant parameters influencing alloy wear resistance in a sliding wear mode.

C. Fractography

Scanning electron microscopy performed on the worn surface of most specimens showed several characteristics common to all. Pits or craters were observed predominantly along the center line of the wear track (Figs. 26-32). Note that the surfaces shown are the tip of a hemispherical pin which has been worn flat. It is interesting to recognize that cuts and grooves normally extensively observed in two or three body abrasive wear were not seen on the surface of any specimens examined in this study. This suggests that a mild sliding or polishing wear regime was established.

Due to the normally low density of craters compared to the total surface area exposed, it is questionable whether the events which formed the craters were the main ones contributing to wear. High magnification examination of the pitted region showed little clear evidence of secondary cracking as would be expected for a crack initiation and propagation mechanism (Fig. 28). Additional high magnification observations of the specimen trailing edge indicated what appears to be a bulk plastic metal flow (see Figs. 26c, 29, 31d, 32c). A step-like appearance of the edge of these trailing "fingers" was typically observed (Figs. 29c, 32c, 32d). It is not clear whether the formation and fracture of these fingers was the major contributor to wear in lieu of the observed crater events.

IV. Discussion

It is often assumed that sliding wear resistance, as abrasive wear resistance, increases as a strong function of initial hardness. The observation of sliding wear resistance being independent of hardness for the experimental alloys and wear resistance decreasing with increasing hardness for the commercial alloys clearly shows the assumption is invalid for this tribological system. Yet, hardness is a complicated second order parameter, as previously mentioned. To gain a better understanding of wear behavior, it is necessary to establish more fundamental relationships. However, material properties such as strength, toughness, and hardening behavior are the product of the microstructure from which they evolve. Thus, it is important to begin with consideration of the microstructural influences on mechanical properties and wear.

It is commonly known that most commercial "wear resistant" materials are comprised of multiphase structures. Optimally, strong second phases are employed to strengthen a soft primary phase, while retaining its toughness. However, the volume, size, and distribution of the second phase critically control the mechanical behavior of the dual phase system. The commercial materials examined in this study were comprised of two or more phases. It appears that the inferior toughness and wear behavior of Astralloy and Firmex, compared to the experimental steels stem from the nonuniform distribution of large carbides and inclusions, respectively, (Fig. 11, 14-17) acting as nucleation sites for failure. Whereas for Abrasaloy, the softest of the

commercial steels, a more uniform distribution of small carbides with little or no large inclusions being present in the bainite-matrix appears to account for its high wear resistance. However, the relatively poor sliding wear behavior of AISI 4340 is difficult to explain in the above manner. It seems that the presence of discontinuous interlath retained austenite may have significantly contributed to its low toughness and wear resistance compared to the experimental alloys.

The predominantly superior wear behavior of the Fe/Cr/C/Mn experimental steels over the commercial alloys appears to be due to the presence of a dislocated lath martensite structure in association with continuous interlath films of retained austenite (Fig. 6). Since little, if any, change was observed in the martensite substructure with increasing additions of Mn up to 2%, previous investigators related the increases in plane strain fracture and notch impact toughness to increases in the volume fraction of retained austenite. As observed in Fig. 20, there is a 25% increase in wear resistance with an increase of 1 to 3% in austenite content as determined by X-ray analysis (2 to 6% by Mössbauer). To confirm this trend, a temper martensite embrittled specimen, having a low austenite content showed good agreement with the established trend. As observed in Fig. 24, the trend of increasing wear resistance with impact energy is, therefore, apparently consistent with the other observations. Hence, the effect of retained austenite on toughness and wear resistance appears to be established, at least in these experimental steels.

Further indication of the effect of retained austenite on wear behavior is seen in Fig. 21. The drop in wear resistance to approximately the same level for both the fine and coarse grained 2% Mn steels after tempering at 300°C is the result of austenite decomposition to precipitate interlath ferrite and cementite (temper martensite embrittlement). T.M.E. has been shown to reduce impact toughness by 50% in these alloys.[42] Although there is further degradation of toughness after tempering at 500°C, inducing temper embrittlement,[67] there is little further loss in wear resistance, even though impurities are known to have segregated to one prior austenite grain boundary. These results appear to imply that the loss of austenite on tempering at 300°C has the most significant effect on wear. Consequently, this is further indication of the effect of retained austenite on wear resistance.

Since there is an apparent empirical relation between retained austenite, toughness, and wear resistance, it is important to discusss the stability of austenite. It has been suggested that austenite is stabilized at room temperature by a combination of: (1) Chemical stabilization[62] in which carbon interstitials segregate to the lath boundaries to lower the local M_s temperature sufficiently below room temperature such that austenite is stable (at room temperature). (2) Thermal stabilization[71,72] is caused by diffusion of carbon and nitrogen to pin dislocations so as to inhibit their motion and prevent stress relaxation in the austenite or martensite. (3) Mechanical stabilization occurs because of platic deformation in the austenite accompanying the shear transformation.[40,65,73,74]

It has also been suggested that indirect benefits of austenite are the high solubility of interstitials, prevention of brittle lath boundary carbides, and the presence of a highly coherent lath boundary interface.[47] Further, it has been indicated[57] that the presence of retained austenite, depending on its mechanical and thermal stabilities, can provide a direct benefit to increased crack propagation resistance through one of a combination of the following mechanisms 1) crack branching 2) crack blunting, and 3) transformation induced plasticity.[52] Although crack branching and crack blunting are plausible, in the present study with such low volume fractions of retained austenite it seems unlikely that trip-induced plasticity would be playing a significant role in determining the toughness. However, the microstructural mechanism by which austenite toughens martensitic steels is not yet well established.

The question of austenite stability is obviously important to the mechanism by which sliding wear occurs. However, little information is available regarding the relative stability of austenite in the Fe/Cr/C alloys. An indication of the austenite instability was derived from a Mössbauer spectrum from the surface of a deformed compact tension specimen (K_{IC}) showing no retained austenite, where originally there was 6%. It is clear the austenite had transformed due to plastic deformation. Although the surfaces of wear specimens were too small to obtain an accurate Mössbauer spectrum or an X-ray scan, the results of the K_{IC} experiment infer little or no retained austenite would exist on the surface of the worn materials, if one assumes there

has been at least as much surface deformation in wear as around the crack tip in performing a K_{IC} test. This appears to be a reasonable assumption, in view of over 50 microns of material being removed by sliding wear. Consequently, one might expect austenite to be converted to 100% martensite in the worn surface and to a finite depth below the surface. It is clear that to understand these effects, it is necessary to consider the wear mechanism.

The observed trend of increasing wear resistance with impact energy and poor correlation with plane strain fracture toughness suggest that both crack initiation and crack propagation behavior are important parameters within the wear mechanism. However, the observed increase in wear resistance with decrease in prior austenite grain size could substantiate the importance of crack initiation behavior to the wear mechanism. Carlson and Ritchie[75] suggest that decreases in prior austenite grain size in the Fe/Cr/C system lead to an increase in the threshold stress intensity factor. Therefore, the smaller the grain size, the more difficult is fatique crack initiation; although possibly coincidental, this may suggest that crack initiation behavior of a material is important in determining its sliding wear resistance.

Since very few secondary cracks were observed on the surface of the wear specimen (Fig. 28), it appears that a mechanism different from the "Delamination Theory" is operative. Scanning electron microscopic observations (Figs. 26-32) of the worn surfaces of many specimens indicate that there are two dominant modes of material

removal: (1) Cratering occurring on the face of the contact plane (as previously discussed); (2) bulk plastic flow of material across the contact surface. Due to relatively low density of craters with respect to exposed surface, the bulk material flow across the worn surface with subsequent fracture off the trailing edge (Figs. 29, 31) appears to be the dominant cause of wear. However, from these observations the microstructural mechanism by which sliding wear occurs is not obvious. Consequently, it is impossible to make any definite statements about relative austenite stability with respect to wear or the reason for increased wear resistance with increasing austenite content without first ascertaining the wear mechanism. It should, therefore, be the purpose of future work to examine cross sections of some worn region under transmission electron microscopy to attempt to determine the role of retained austenite with respect to wear. Transformation extent and mode of "wear failure" initiation would be the principles addressed to attempt to elucidate the wear mechanism.

V. Conclusions

1. Micro-duplex structures of dislocated lath martensite with continuous interlath films of retained austenite appear to be excellent combinations for high sliding wear resistance as well as for strength and toughness.

2. Hardness, toughness, and microstructure appear to be mutually important for determining sliding wear resistance.

3. Refinement of prior austenite grain size increased sliding wear resistance.

4. The grain refined Fe/4Cr/.3C/2Mn experimental steel exhibits sliding wear resistance superior to all experimental and commercial alloys examined.

5. There appears to be an increasing trend of wear resistance with Charpy V-notch impact energy which may suggest crack initiation behavior is controlling this form of wear.

6. The sliding wear mechanism is not yet known, but clearly should be the subject of future work.

ACKNOWLEDGEMENTS

The author wishes to sincerely thank Professor Gareth Thomas for his support and guidance throughout this investigation. Deep appreciation is extended to Dr. B.V. Narasimha Rao and Mehmet Sarikaya for their patience, encouragement, and many instructive discussions.

The author also wishes to thank Professors Iain Finnie and J.W. Morris, Jr. for their constructive criticism during the course of this work and for their critical review of the manuscript.

Assistance provided by the support staff of the Materials Science and Molecular Research Division of Lawrence Berkeley Laboratory is gratefully acknowledged. In particular, the assistance provided by Weyland Wong, Duane Newhart, John Holthuis, Don Kreiger, and Sandy Stewart was sincerely appreciated. Special thanks are also due to Brent Fultz for kindly performing Mössbauer spectrographic determinations of the retained austenite content in the materials studied.

Finally, the author wishes to thank his wife, Terri, for her unfailing support, cooperation, understanding, and companionship which will forever be appreciated.

This work was done under the support of the Division of Material Science, Office of Basic Energy Sciences, U.S. Department of Energy through the Materials and Molecular Research Division of the Lawrence Berkeley Laboratory under Contract No. W-7405-Eng-48.

Appendix I

The Mössbauer effect is a nuclear γ-ray resonance phenomenon which involves a recoilless γ-ray emission from a radiation source and a recoiless absorption process by a specific nucleus; Fe^{57} in this case. The information present in a Mössbauer spectrum reflects electric and magnetic environments present at Fe^{57} nuclei in the absorber material. In the specimens used in this research, the martensite phase gave a magnetically split spectrum which did not overlap with the absorption peaks from the paramagnetic austenite and carbide phases. γ-rays, 14.4 eV, re-emitted by the absorber were counted to accumulate the spectra.[52] These γ-rays originated from Fe^{57} nuclei less than 10μm below the square centimeter of specimen surface irradiated. The intensity of paramagnetic and ferromagnetic peaks should be approximately proportional to the number of Fe^{57} nuclei in each phase, but the raw data were corrected for thickness broadening effects.[76]

Since the Mössbauer effect yields information about the fraction of atomic nuclei in a particular excited state, it has been used to quantitatively determine amounts of a particular phase present in a microstructure. However, we are determining the atomic percent of such a phase as austenite present. Since the atomic volume of austenite in a mild steel is approximately 1, no correction of Mössbauer information is necessary to express the amounts of austenite in terms of volume fraction. The Mössbauer data presented in this paper were expressed in volume fraction in light of this approximation.

References

1. D.E. Nass, "Steel Grinding Media used in the United States and Canada," Symposium on Materials for the Mining Industry, Vail, Colorado, 1974, p.173.
2. O. Vignsbo: Proceedings, "Wear of Materials, 1979," Int'l. Conf. on Wear of Materials, 1979, Dearborn, MI, ASME, pp.620-635.
3. F.P. Bowden and D.A. Tabor: "Friction and Lubrication," Methuen and Co., Ltd., London, 1967.
4. D. Tabor: Proceedings, "Wear of Materials, 1977," Int'l. Conf. on Wear of Materials, St. Louis, MO, 1977, ASME, pp.1-11.
5. J.F. Archard: J. Appl. Phys. 1953, 24, pp.981-988.
6. J.F. Archard: J. Appl. Phys. 1961, 52, pp.1420-1425.
7. E.T. Finkin: Wear, 1972, 21, pp.103-114.
8. J. Halling: Wear, 1975, 34, pp.239-244.
9. N. Soda, Y. Kimura, and T. Tanaka: Wear, 1976, 40, pp.23-25.
10. Y. Tsuya: Technical Report of Mechanical Engineering Laboratory No. 81 (in English) Tokyo, Japan, 1976.
11. E. Rabinowicz: "Friction and Wear of Materials," John Wiley and Sons, New York, 1965.
12. E. Rabinowicz: Wear, 1977, 42, pp.149-156.
13. I. Ming Feng: J. Appl. Phys., 1952, 23, p.1011.
14. I. Ming Feng: J. Appl. Phys., 1955, 26, pp.24-32.
15. M. Cocks: J. Appl. Phys. 1962, 33, pp.2152-2161.
16. M. Cocks: J. Appl. Phys. 1964, 35, pp.1807-1814.
17. M. Antler: Wear, 1964, 7, pp.181-203.

18. A.A. Torrance: Wear, 1978, 50, pp.169-182.

19. J.P. Hirth and D.A. Rigney: Wear, 1976, 39, pp.133-141.

20. D.A. Rigney and J.P. Hirth: Wear, 1979, 53, pp.345-359.

21. H.L. Hsu, T.M. Ahro, and D.A. Rigney: Proceedings: "Wear of Materials," ASME, Dearborn, MI, April 1979, pp.12-26.

22. L.A. Mitchell and C. Osgood: Wear, 1976, 40, pp.203-222.

23. A.W. J. deGee: Int'l. Met. Rev., 1979, 2, pp.57-67.

24. J.J. Bikerman: Wear, 1976, 39, pp.1-13.

25. N.P. Suh: Wear, 1973, 25, pp.111-124.

26. N.P. Suh: Wear, 1977, 44, pp.1-16.

27. S. Jaranmir and N.P. Suh: Wear, 1977, 44, pp.39-56.

28. N.P. Suh, N. Saka, and S. Jahdanmir: Wear, 1977, 44, pp.127-134.

29. J.R. Fleming and N.P. Suh: Wear, 1977, 44, pp.39-56.

30. D.E. Diesburg and F. Borik: "Materials for the Mining Industry," Climax Molybdenum Company, USA, 1974, p.15.

31. M.S. Bhat, V.F. Zackay, and E.R. Parker: Proceedings: "Wear of Materials," ASME, Dearborn, MI, April 1979, p.286-290.

32. E. Horbogen: Wear, 33, 1975, p.251-259.

33. G. Thomas: Iron and Steel Int'l., 1973, Vol. 46, p.451.

34. S.K. Das and G. Thomas: Trans. ASM, 1969, 62, p.659.

35. D.H. Huang and G. Thomas: Met. Trans., 1971, 2, p.1587.

36. M. Raghavan and G. Thomas: Met. Trans., 1971, 2, p.3433.

37. I. Lin Cheng and G. Thomas: Met. Trans., 1972, 3, p.503.

38. J. McMahon and G. Thomas: Proc. 3rd Intern. Conf. on Strength of Metals and Alloys, Inst. of Metals, London, 1973, 1, p.180.

39. R.A. Clark and G. Thomas: Met. Trans., 1975, 6A, p.969.

40. B.V.N. Rao and G. Thomas: Mat. Sci. and Eng., 1975, 20, p.195.

41. G. Thomas: Batelle Colloquium on Fundamental Aspects of Structural Alloy Design, R.I. Jaffee and B.A. Wilcox, eds., Plenum Publ. Co., 1977.

42. B.V.N. Rao: Ph.D. Thesis, University of California, Berkeley, February, 1978, LBL Report No. 7361. (For X-ray data see Ref. 53).

43. M. Sarikaya: M.S. Thesis, University of California, Berkeley, June 1979, LBL Report No. 9260.

44. T.H. Rabe: M.S. Thesis, University of California, Berkeley, June 1979, LBL Report No. 9262.

45. B. Steinberg: M.S. Thesis, University of California, Berkeley, June 1979, LBL Report No. 9103.

46. G. Thomas: Met. Trans., 1978, 9A, pp.439-450.

47. B.V.N. Rao and G. Thomas: April 1979, LBL Rerport No. 9337.

48. M. Carlson: M.S. Thesis, University of California, Berkeley, 1978, LBL Report No. 7670.

49. M.F. Carlson, B.V.N. Rao and G. Thomas: Met. Trans., 1979, 10A, pp.1273.

50. J. Koo, B.V.N. Rao and G. Thomas: LBL Preprint No. 8922, April 1979 (published in Metals Progress, September 1979).

51. R. Bill and D. Wisander: Wear, 1977, 41, p.351-363.

52. B. Fultz: M.S. Thesis, University of California, Berkeley, June 1978, LBL Report No. 7671.

53. B.V.N. Rao and G. Thomas: Met. Trans., 1980, 11A, p.441.

54. R.L. Miller: Trans. ASM, 1964, 57, p.893.

55. G.Y. Lai, W.E. Wood, R.A. Clark, V.F. Zackay, and E.R. Parker: Met. Trans., 1974, 5, p.1663.

56. E. Parker and V. Zackay: Eng. Fract. Mech., 1975, 7, p.371.

57. R. Horn and R.O. Ritchie: Met. Trans., 1978, 9A, p.1039.

58. R.O. Ritchie, B. Francis, W.L. Server: Met. Trans., 1976, 7, p.831.

59. L.H. Van Vlack, Material Science for Engineers, Addison Wesley Publ. Co., 1970.

60. H.T. Angus: Wear, 1979, 54, pp.33-78.

61. G. Thomas: Met. Trans., 1972, 2, p.2373.

62. G.R. Speich and W.C. Leslie: Met. Trans., 1972, 3, p.1043.

63. R.F. Heheman, K.R. Kinsman and H.I. Aaronson: Met. Trans., 1972, 3, p.1077.

64. K.J. Irvine, F.B. Pickering and J. Garstone: JISI, 1960, 196, p.65.

65. P.M. Kelly and J. Nutting, JISI, 1961, 183, p.199.

66. J.D. Bolton, E.R. Petty and G.B. Allen: Met. Trans., 1971, 2, p.2912.

67. G. Thomas and B.V.N. Rao: Intern. Conf. on "Martensitic Transformation," Kiev, USSR, 1977.

68. B.V.N. Rao: University of California, Berkeley, July 1978, LBL Report No. 8013.

69. R.P. Brobst and G. Krauss: Met. Trans., 1974, 5, p.457.

70. W.C. Leslie and R.L. Miller: Trans. ASM, 1964, 57, p.972.

71. P.G. Shewmon: "Transformation in Metals," McGraw-Hill Book Co., 1969.

72. G.S. Ansell, S.J. Donachie, and R.W. Messler, Jr.: Met. Trans., 1971, 2, p.2443.

73. B. Edmondson and T. Ko: Acta Met., 1957, 2, p.235.

74. H.K.D.H. Badeshia and D.V. Edmonds: Proceedings: "International Conference on Martensitic Transformations," Cambridge, MA, p.28.

75. M. Carlson and R. Ritchie: Acta Met., 1977, 11, p.1113.

76. B. Fultz and J.W. Morris, Jr.: submitted to J. Appl. Physics, May 1980.

TABLE 1

STEEL COMPOSITION

EXPERIMENTAL ALLOY	C	Cr	Mn	Ni	Mo	Co	Si	Ti	V	Fe
Fe/4Cr/.3C	0.29	4.00	----	----	----	----	----	----	----	Bal.
Fe/4Cr/.3C/1Mn	0.24	4.10	1.0	----	----	----	----	----	----	Bal.
Fe/4Cr/.3C/2Mn	0.25	4.00	1.93	----	----	----	0.07	----	----	Bal.
Fe/4Cr/.3C/5Ni	0.27	3.8	----	5.00	----	----	----	----	----	Bal.
INDUSTRIAL ALLOYS										
Abrasalloy	0.35	0.45	0.87	0.58	0.14	----	0.20	----	----	Bal.
Astralloy	0.29	1.67	1.07	3.68	0.37	0.08	0.42	0.007	.01	Bal.
Firmex	0.26	0.30	1.94	0.73	0.24	----	0.57	0.06	----	Bal.
Aisi 4340	0.40	0.70	0.75	1.75	0.25	0.02	0.02	----	.01	Bal.

TABLE 2A

COARSE GRAINED EXPERIMENTAL ALLOYS
MECHANICAL PROPERTIES AND WEAR DATA

ALLOY	TEMPERING TEMP. (°C)	YS (KSI)	UTS (KSI)	% REDUCTION AREA	% TOTAL ELONGATION (UNIFORM)	K_{IC} KSI$\sqrt{IN}$	CHARPY V-NOTCH FT-LB	HARDNESS (R_C)	AVERAGE FRICTION COEFFICIENT	AVERAGE WEAR RESISTANCE (mm/mm^2)x10^6
Fe/4Cr/.3C	AQ	195	240	35.4	8.0	71	18	52.0	--	--
	200	189	230	45.4	11.0	76.5	30	48.5	--	--
Fe/4Cr/3C/1Mn	AQ	198	240	28.5	6.4	85.5	11.5	51.0	--	--
	200	185	224	45.7	10.0	-----	48.0	44.6	--	--
Fe/4Cr/.3C/2Mn	AQ	207	265	33.0	8.5	59	3.4	53.1	0.46	6.92
	200	195	235	36.0	6.5	180*(126)	40.0	47.8	0.49	6.84
	300	177	212	19.0	---	-----	18.5	42.0	0.55	5.34
	500	150	175	24.0	12.5	-----	4.0	37.0	0.50	5.24
Fe/4Cr/.3C/5Ni	AQ	195	275	25.0	9.0	89.5	19.5	----	-----	-----
	200	187	234	----	12.0	123.0	43.5	45.8	.72	5.47

* Violated plane strain conditions. Calculated K_Q instead of K_{IC}.

TABLE 2B

FINE GRAINED EXPERIMENTAL ALLOYS
MECHANICAL PROPERTIES AND WEAR DATA

ALLOY	TEMPERING TEMP. (°C)	YS (KSI)	UTS (KSI)	% REDUCTION AREA	% TOTAL ELONGATION (UNIFORM)	K_{IC} KSI$\sqrt{IN}$	CHARPY V-NOTCH FT-LB	HARDNESS (R_C)	AVERAGE FRICTION COEFFICIENT	AVERAGE WEAR RESISTANCE (mm/mm^2)x10^6
Fe/4Cr/.3C	AQ	180	230	24.0	9.4	66.0	20.0	47.5	----	----
	200	187	227	32.0	9.0	----	20.5	47.2	0.48	6.67
Fe/4Cr/.3C/1Mn	AQ	177	228	47.4	13.7	85.0	29.1	43.7	----	----
	200	185	223	50.0	13.9	110.0	40.0	43.6	0.46	6.46
Fe/4Cr/.3C/2Mn	AQ	189	242	38.7	11.0	84.0	30.5	47.5	0.60	7.27
	200	184	230	50.8	15.4	180*(126)	49.5	47.5	0.60	8.68
	300	182	215	58.5	14.6	---	29.5	45.3	0.54	5.70
Fe/4Cr/.3C/5Ni	AQ	200	280	44.5	11.1	75.0	27.0	49.1	----	----
	200	193	242	57.5	15.8	102.0	41.7	47.8	0.72	7.71

* Violated plane strain conditions. Calculated K_Q instead of K_{IC}.

TABLE 3

INDUSTRIAL ALLOYS

ALLOY	YS (KSI)	UTS (KSI)	% REDUCTION AREA	% TOTAL ELONGATION (UNIFORM)	K_{IC} KSI$\sqrt{IN}$	CHARPY V-NOTCH FT-LB	HARDNESS (R_C)	AVERAGE FRICTION COEFFICIENT	AVERAGE WEAR RESISTANCE (mm/mm^3)$\times 10^6$
Abrasaloy	175	180	45	12	*	*	34-38	0.53	7.89
Astralloy	157	241	39	11-12	*	31.2	45	0.48	4.09
Firmex	184	198	50	10-12	*	15	39.5	0.50	5.44
AISI 4340	225	290	13	7	45	13	52	0.67	3.70

*Information not available from manufacturer.

Figure Captions

Fig. 1 Illustration of heat treatments employed in this study.

Fig. 2 Schematic drawing of the microstructure produced by employing heat treatments to Mn and Ni steels.

Fig. 3 Sketch of wear specimen preparation from heat treated steel blank.

Fig. 4 Front view of wear machine used in this study.

Fig. 5 Close up of wear machine showing typical wear track, pin specimen, deadweight load, and strain gauges.

Fig. 6 Transmission electron micrographs of 2% Mn alloy; (a) bright field shows dislocated lath martensite; (b) dark field shows continuous interlath films of retained austenite (courtesy of Dr. B.V.N. Rao).

Fig. 7 Transmission electron micrographs of 2% Mn steel after 200°C tempering:

(a) bright field showing Widmanstatten cementite;

(b) dark field of cementite particles;

(c) diffraction pattern with superimposed aperture;

(d) indexed diffraction pattern (courtesy of Dr. B.V.N. Rao).

Fig. 8 Transmission electron micrograph of 2% Mn steel after 300°C tempering:

(a) bright field;

(b) dark field--austenite has decomposed to ferrite and interlath cementite. Arrows indicate cementite plates (courtesy of M. Sarikaya).

Fig. 9 Comparison of Mössbauer spectroscopy obtained in this study to x-ray diffraction obtained in a previous study[42] by Miller's method[52] for determination of small volume fractions of retained austenite. Mössbauer appears to be more effective in resolving small quantities of retained austenite than x-ray diffraction.

Fig. 10 Optical and scanning electron microscopic (SEM) observations on the commercial materials:

(a) optical--Astralloy has a fine structure, not well resolved optically;

(b) SEM--on an etched optical specimen shows either bainite or martensite;

(c) Abrasaloy--larger prior austenite grain size than Astralloy;

(d) SEM--prior austenite grain boundaries are visible on this etched optical specimen.

Fig. 11 Optical and scanning electron microscopic observations of Firmex:

(a) optical--inclusions are oriented parallel to rolling direction (indicated by arrow);

(b) and (c) SEM image and sulphur x-ray map show inclusions to be sulphur rich, most probably MnS.

Fig. 12 Transmission electron micrograph of Abrasaloy:

(a) bright field;

(b) dark field of Fe_3C spot showing intra and interlath carbides. Inset shows S.A.D. in which carbide reflections

carbides. Inset shows S.A.D. in which carbide reflections are clearly indicated.

Fig. 13 Transmission electron micrograph of Abrasaloy:

(a) bright field;

(b) dark field of cementite spot showing intra- and inter-lath cementite particles.

Fig. 14 Transmission electron micrograph of Astralloy:

(a) bright field showing martensite;

(b) dark field for which martensite has been imaged. Small carbides are seen in background.

Fig. 15 Transmission electron micrograph of Astralloy:

(a) bright field exhibiting the observed microtwins. These were observed periodically throughout the structure;

(b) selected area diffraction pattern.

Fig. 16 Transmission electron micrograph of Firmex:

(a) bright field of several laths containing Widmanstatten cementite;

(b) dark field of carbide reflection showing extent of precipitation. Inset shows selected area diffraction pattern.

Fig. 17 Transmission electron micrograph of Firmex:

(a) bright field showing martensite laths;

(b) bright field of another area of the specimen showing carbide precipitation.

Fig. 18 Wear resistance as a function of time for the 2% Mn, fine grained experimental steel as well as a commercial alloy

Abrasaloy. Time in this case reflects distance travelled.

Fig. 19 Wear resistance is shown to decrease with increasing prior austenite grain size.

Fig. 20 Increasing trend of wear resistance with volume fraction retained austenite. Volume fraction retained austenite was determined by x-ray analysis. Substructural twinning in the martensite appears to be detrimental to wear resistance as is observed for the 5% Ni alloy. (Volume fraction retained austenite determined by x-ray analysis).

Fig. 21 Wear resistance versus tempering temperature shows that temper martensite embrittlement (occurring ~ 300°C) leads to a considerable drop in wear resistance, but temper embrittlement (occurring at 500°C) does not further degrade wear characteristics.

Fig. 22 Wear resistance as a function of hardness shows a decreasing trend of wear resistance with increasing hardness for commercial material. However, for the experimental steels wear resistance is independent of hardness.

Fig. 23 Wear resistance shows a poor correlation to plane strain fracture toughness.

Fig. 24 Wear resistance versus Charpy notch impact energy shows a good correlation and suggests that crack initiation may play an important role in determining wear resistance.

Fig. 25 Bar graph indicating superior nature of Quatough to industrial alloys tested. The air melted alloy shows significant promise.

Fig. 26 Fractographs of worn wear pin surface of double heat treated Fe/Cr/C base alloy;

(a) low magnification view of worn surface;

(b) center of loading area;

(c) trailing part of surface;

(d) leading part of surface;

(e) "finger-like" protrusions showing evidently "laminar" metal flow has occurred across the worn surface.

Fig. 27 Worn surface of double heat treated 2% alloy (Quatough):

(a) low magnification view of worn surface;

(b) center of loading;

(c) shows low crater density with scattered wear debris;

(d) close-up of typical crater showing evolution of plate-like wear particles.

Fig. 28 Worn surface of double heat treated 2% Mn steel:

(a) general area to show where (b) was taken from;

(b) shows what "appears" to be the production of a wear particle and the corresponding microcracks shown by arrows.

Fig. 29 Worn surface of double heat treated 2% Mn steel:

(a) trailing edge of worn surface;

(b) higher magnification to show area from which (c) was taken;

(c) trailing edge of worn surface shows evidence of plate-like metal removal which is perhaps evidence of metal flow.

Fig. 30 Worn surface of temper martensite embrittled double heat treated 2% Mn steel:

(a) typical worn surface;

(b) angular pits are formed in this alloy as opposed to rounded pits in 200°C tempered-material.

Fig. 31. Worn surface of fine grained, temper martensite embrittled 2% Mn steel:

(a) overview of worn surface;

(b) enlarged section of central loading zone;

(c) trailing edge showing angularity of craters;

(d) typical trailing finger. Cracks leading to fracture of these fingers are apparent. Apparent sheet-like removal of material.

Fig. 32 Worn surface of double heat treated 5% Ni alloy:

(a) typical worn surface showing extensive length of trailing fingers of metal;

(b) center of load;

(c) close-up of trailing "finger" which is somewhat oxidized (small growths on surface) but it exhibits the "plate-like metal" flow observed on other materials.

HEAT TREATMENT SCHEDULE

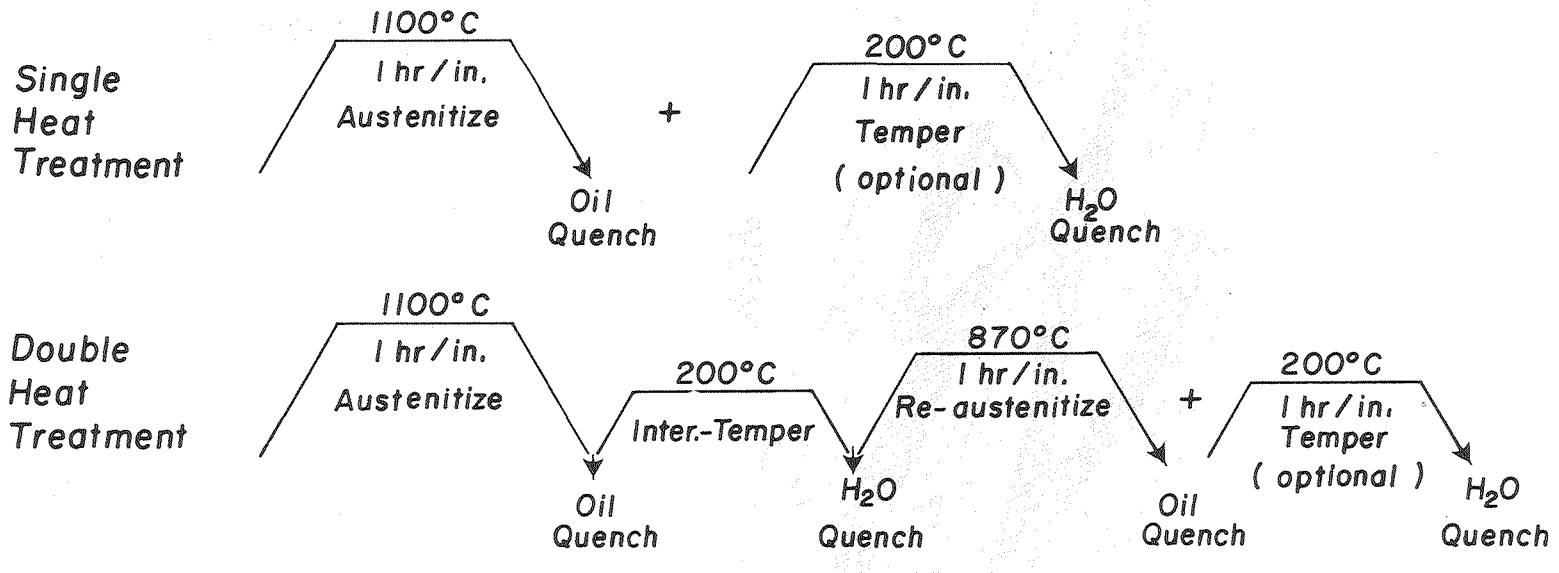

XBL802-321

Fig. 1

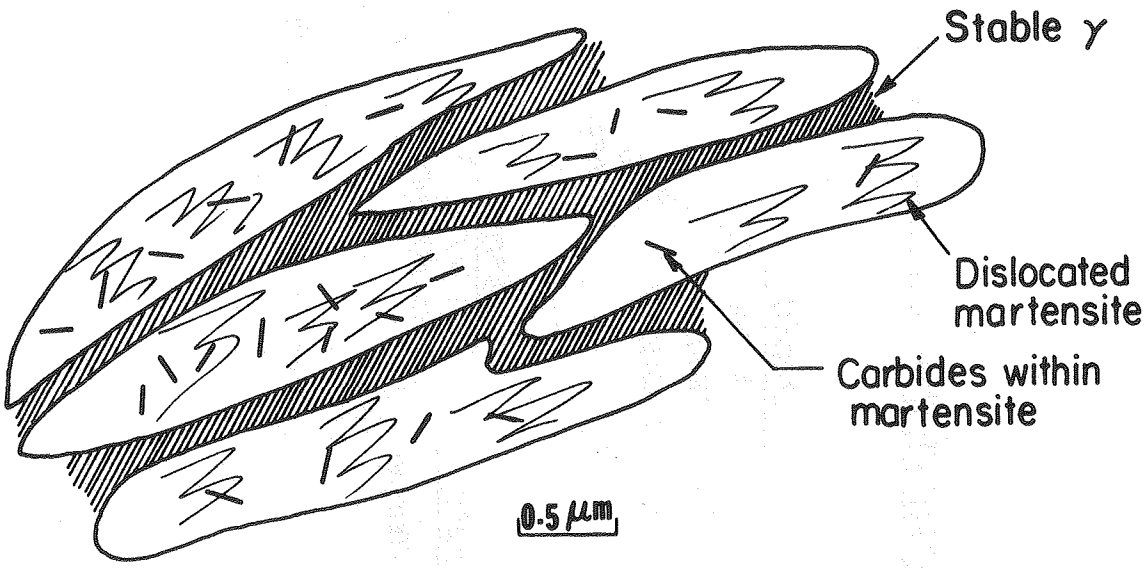

XBL 7711-10457

Fig. 2

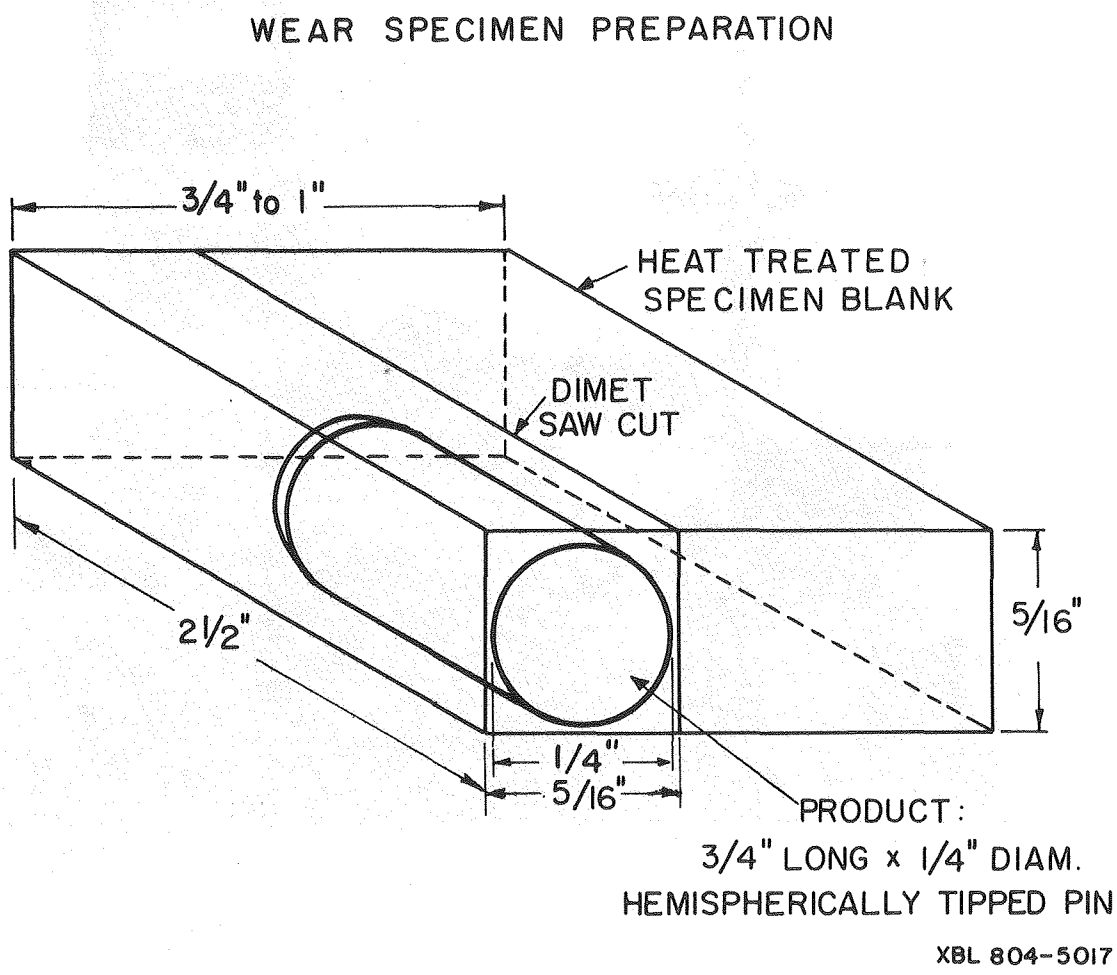
WEAR SPECIMEN PREPARATION
3/4" to 1"
HEAT TREATED
SPECIMEN BLANK
DIMET
SAW CUT
2 1/2"
5/16"
1/4"
5/16"
PRODUCT:
3/4" LONG x 1/4" DIAM.
HEMISPHERICALLY TIPPED PIN
XBL 804-5017

Fig. 3

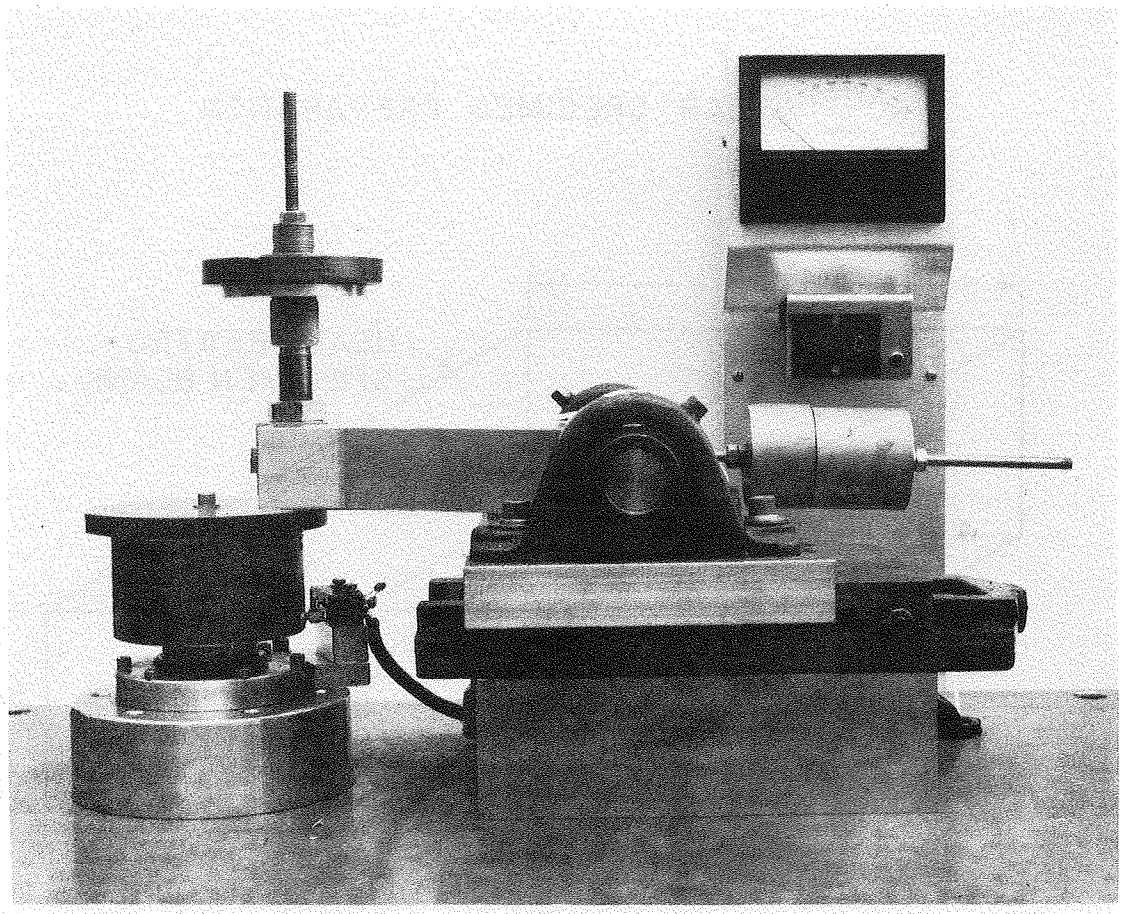

CBB 790 14749

Fig. 4

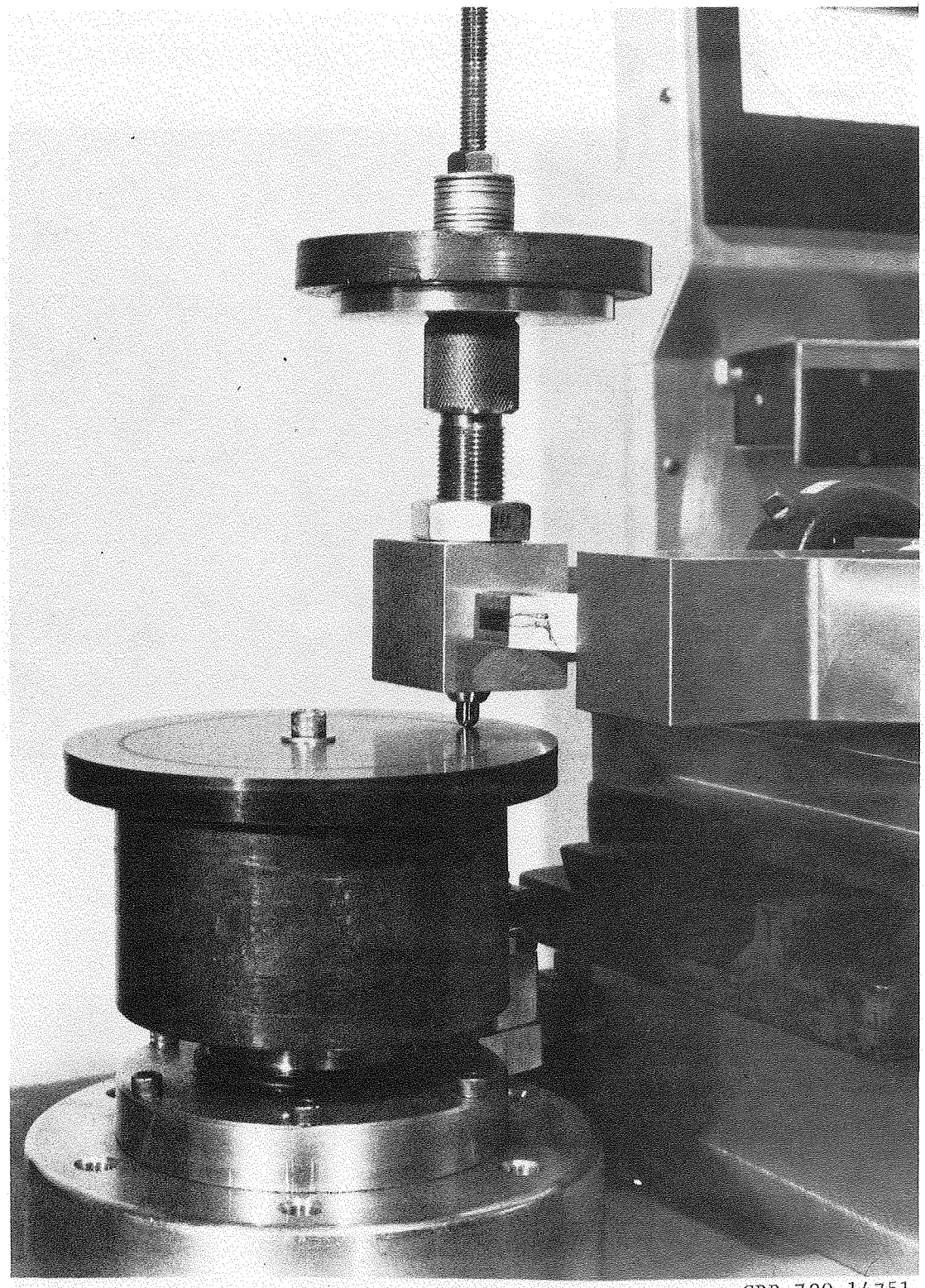

CBB 790 14751

Fig. 5

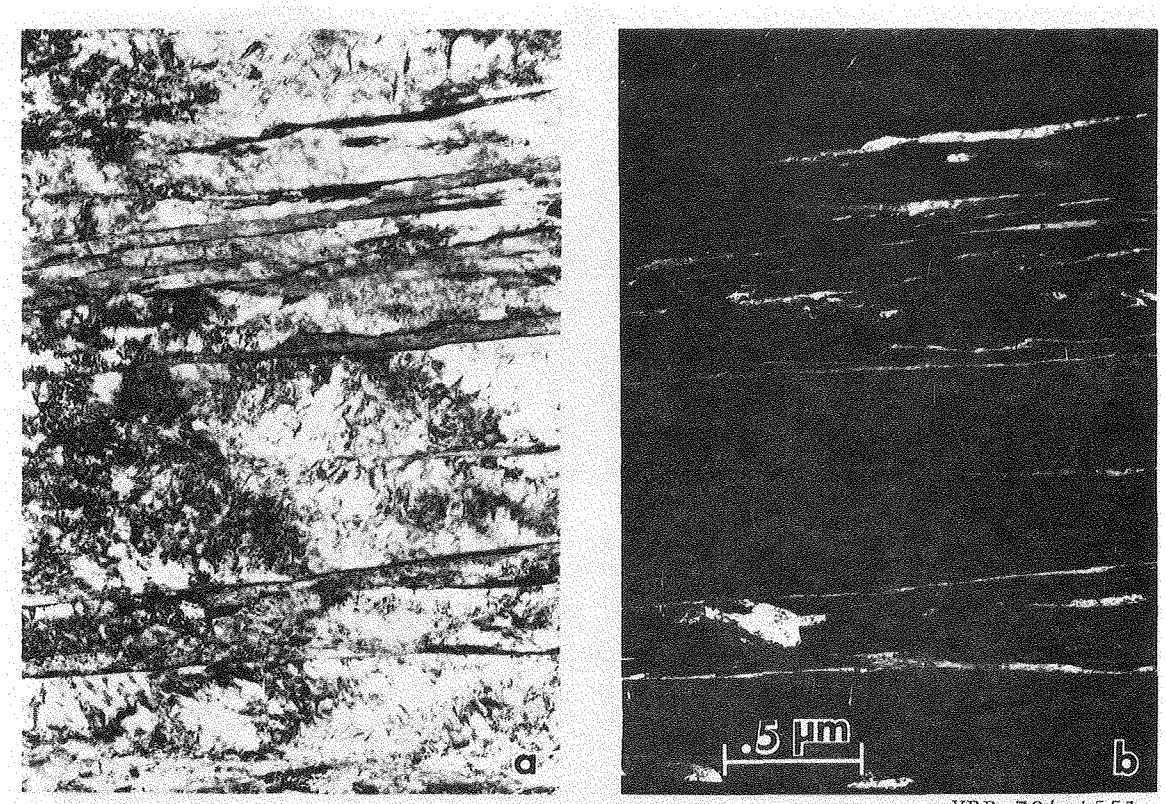

XBB 794 4551

Fig. 6

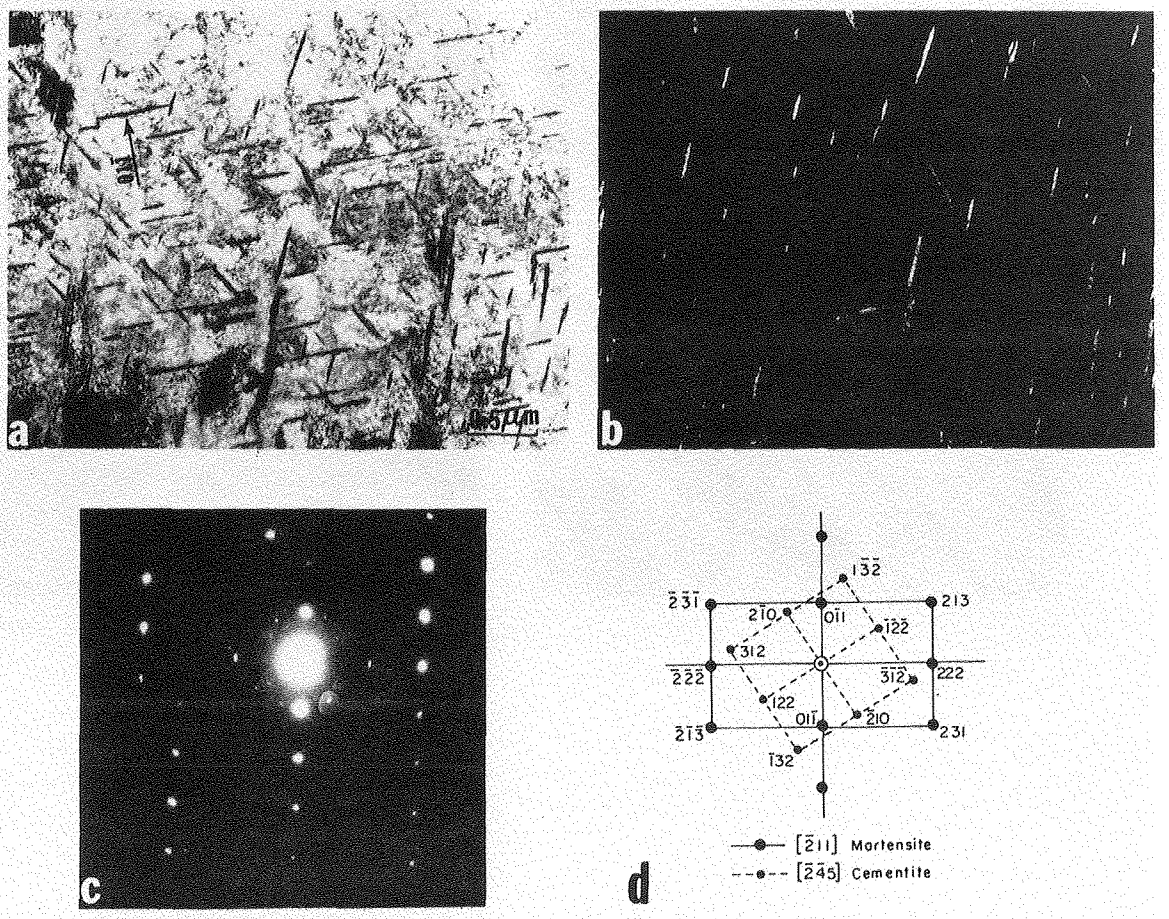

XBB 782 1175

Fig. 7

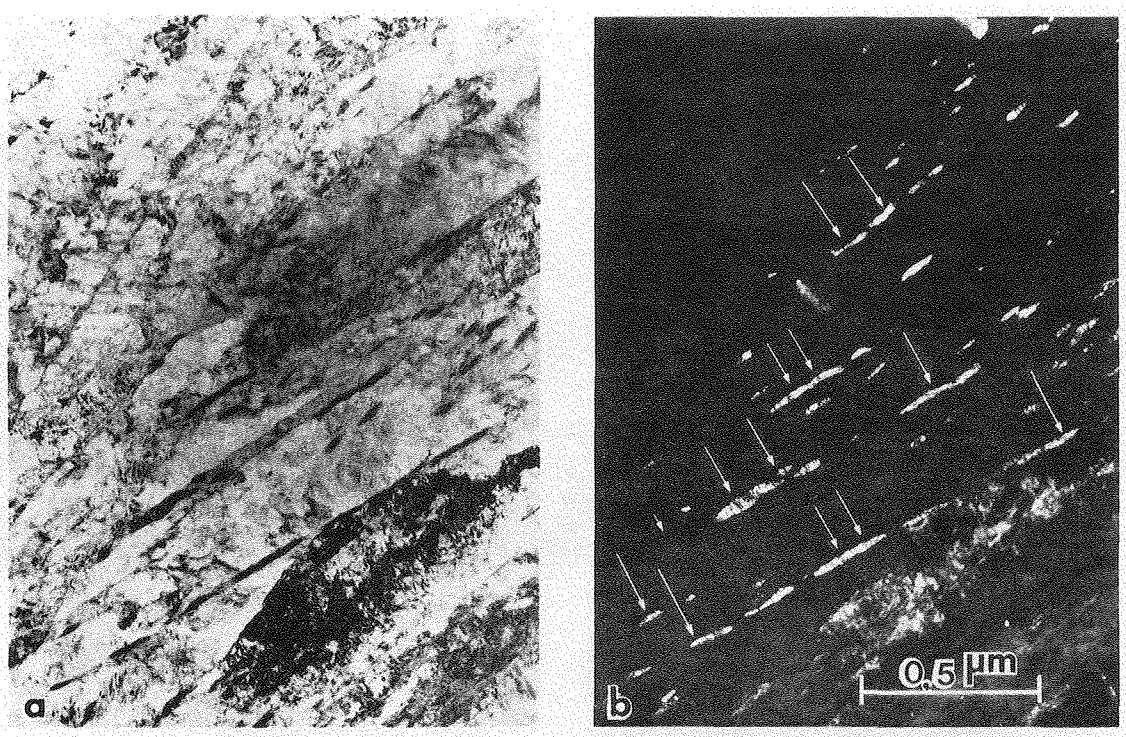

XBB 794 5669

Fig. 8

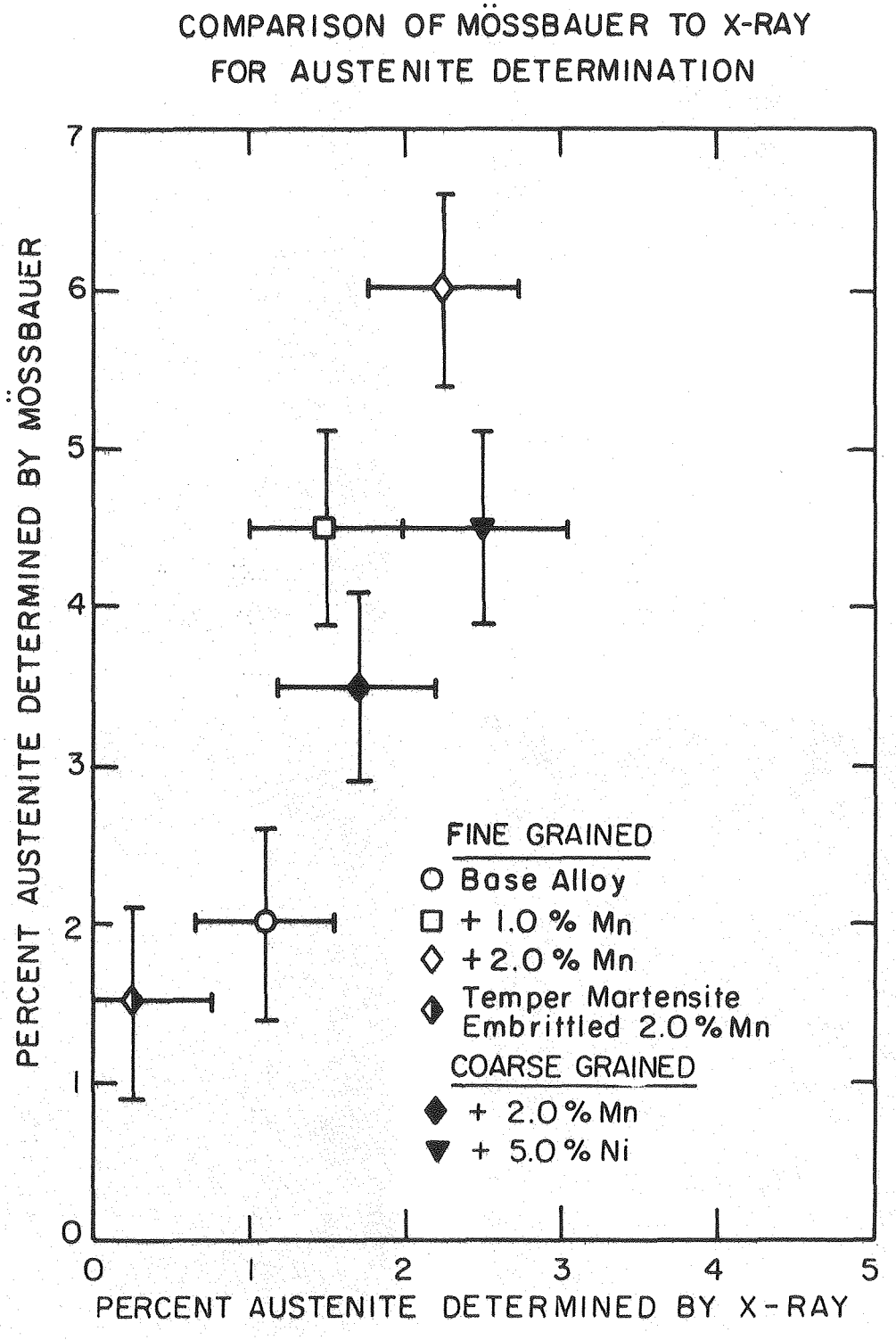
COMPARISON OF MÖSSBAUER TO X-RAY
FOR AUSTENITE DETERMINATION
PERCENT AUSTENITE DETERMINED BY MÖSSBAUER
PERCENT AUSTENITE DETERMINED BY X-RAY
0
1
2
3
4
5
6
7
FINE GRAINED
Base Alloy
+ 1.0 % Mn
+ 2.0 % Mn
Temper Martensite Embrittled 2.0 % Mn
COARSE GRAINED
+ 2.0 % Mn
+ 5.0 % Ni
XBL 805-5192

Fig. 9

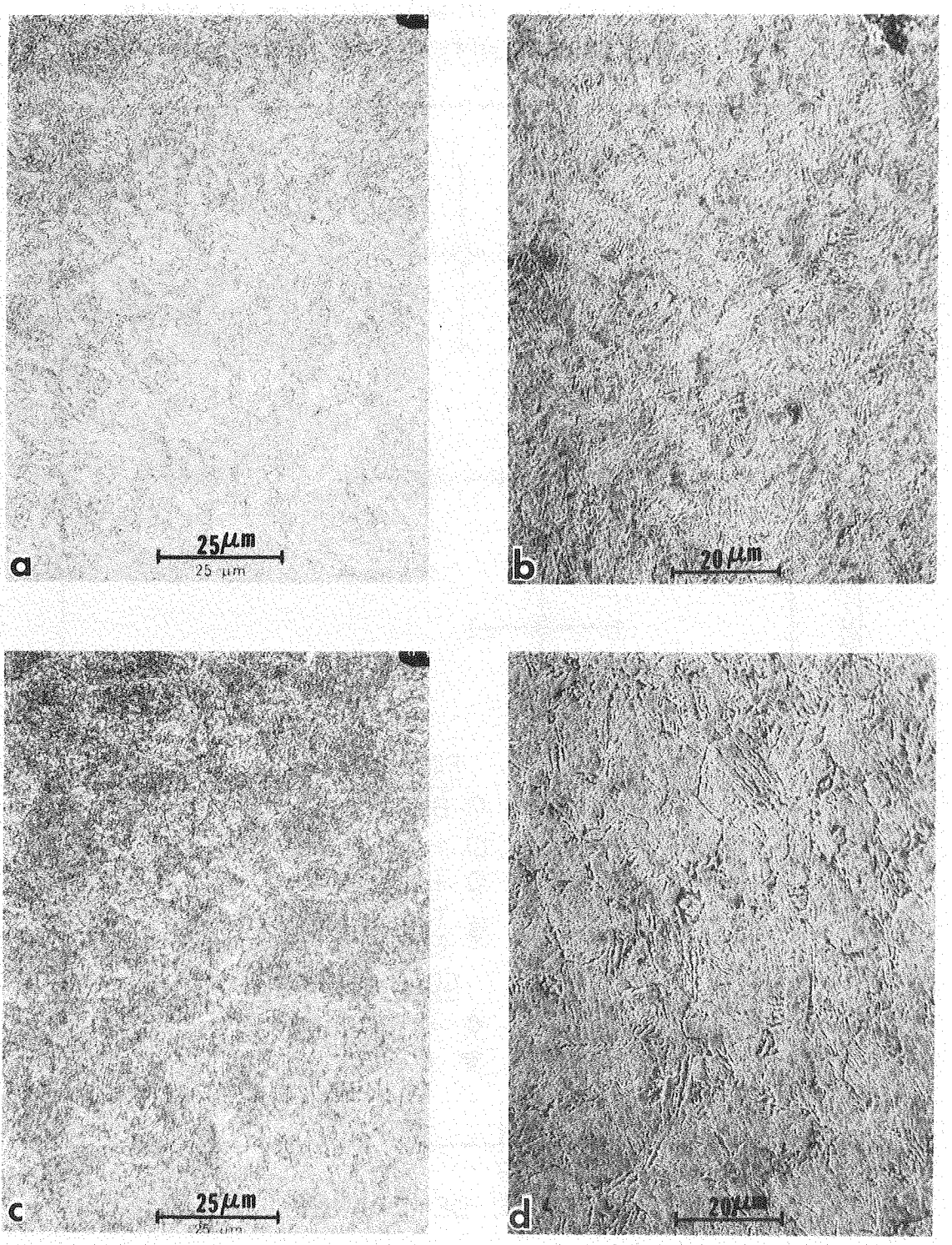

XBB 805 5767

Fig. 10

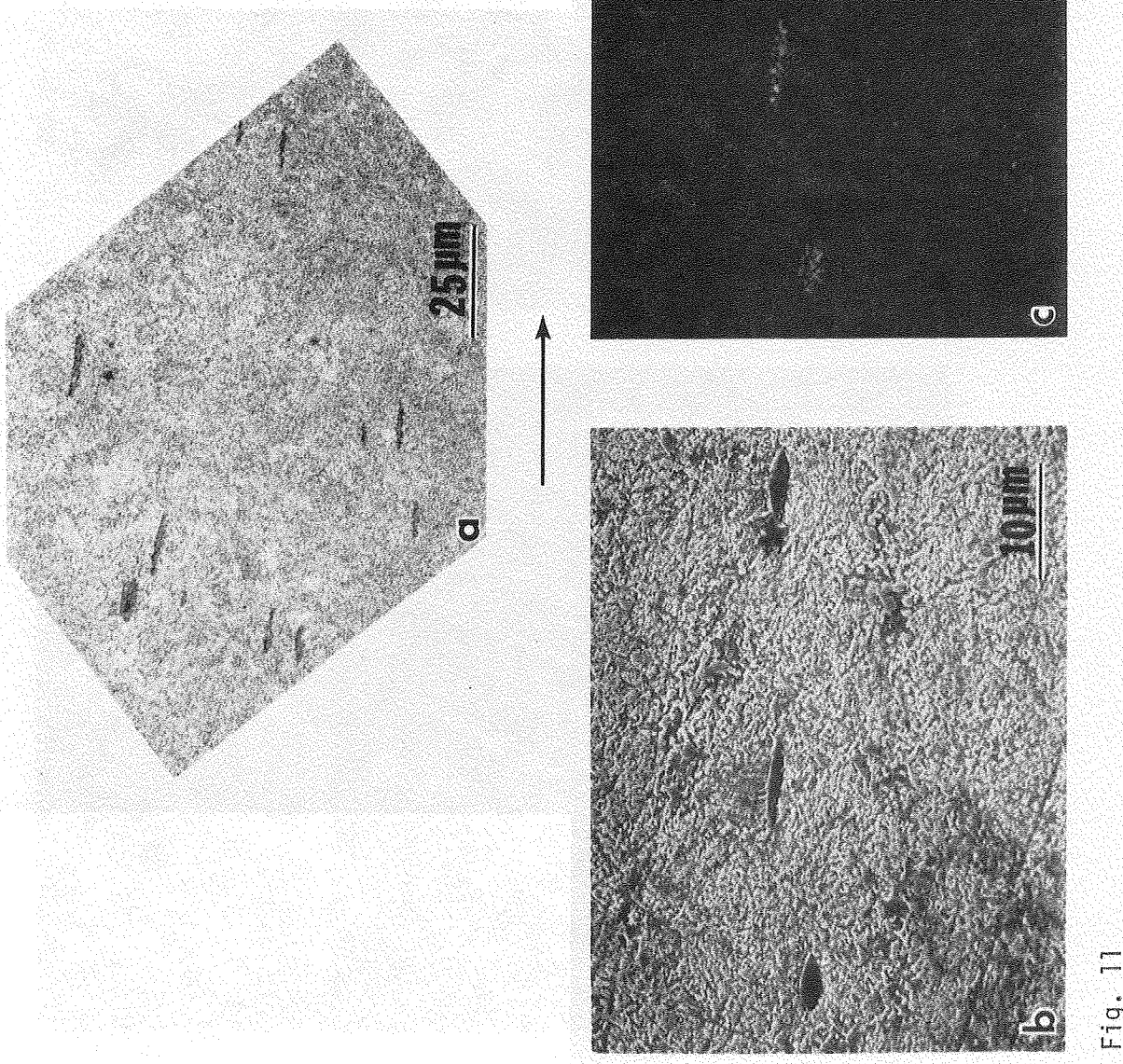

XBB 805 5765

Fig. 11

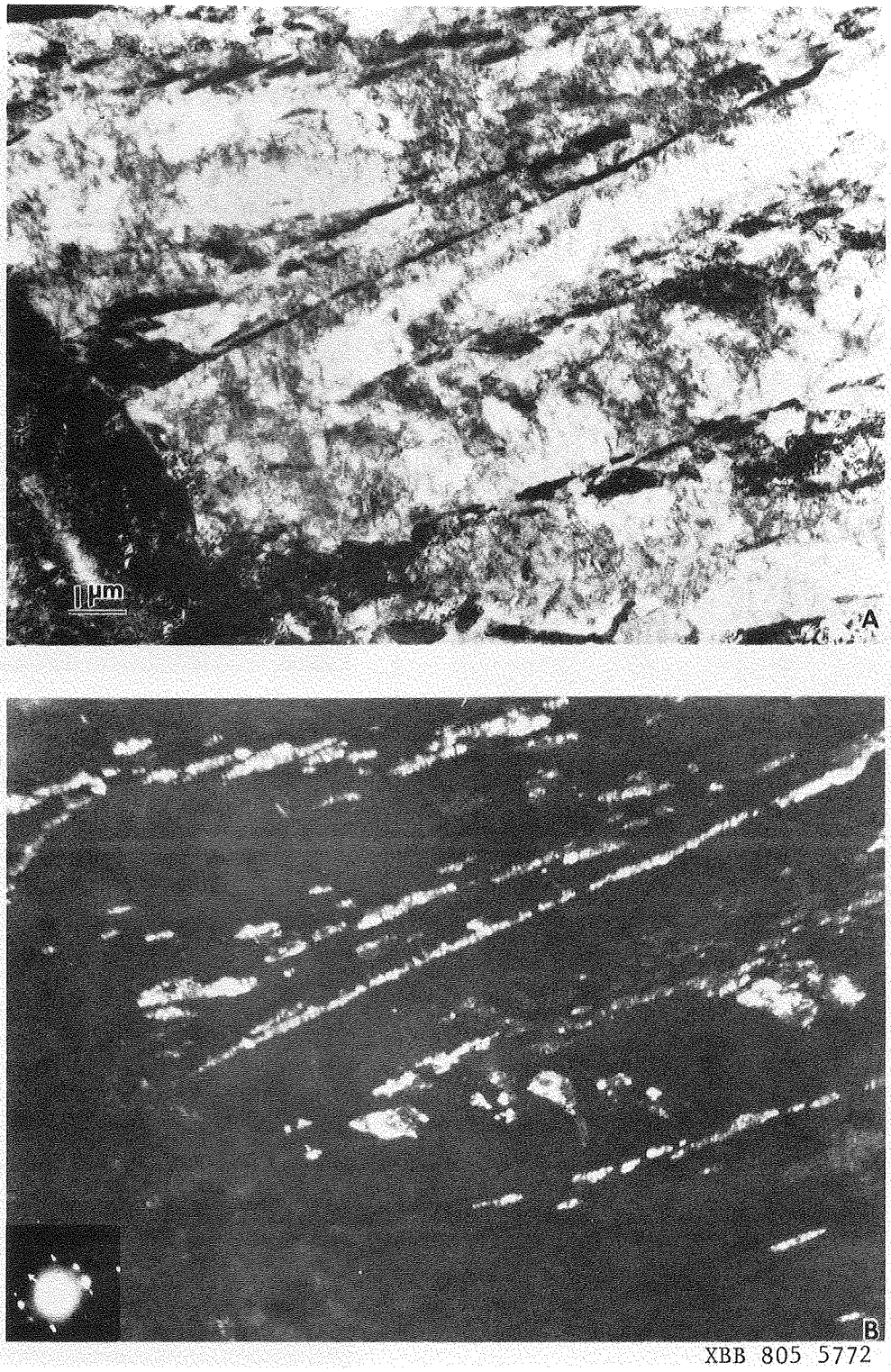

XBB 805 5772

Fig. 12

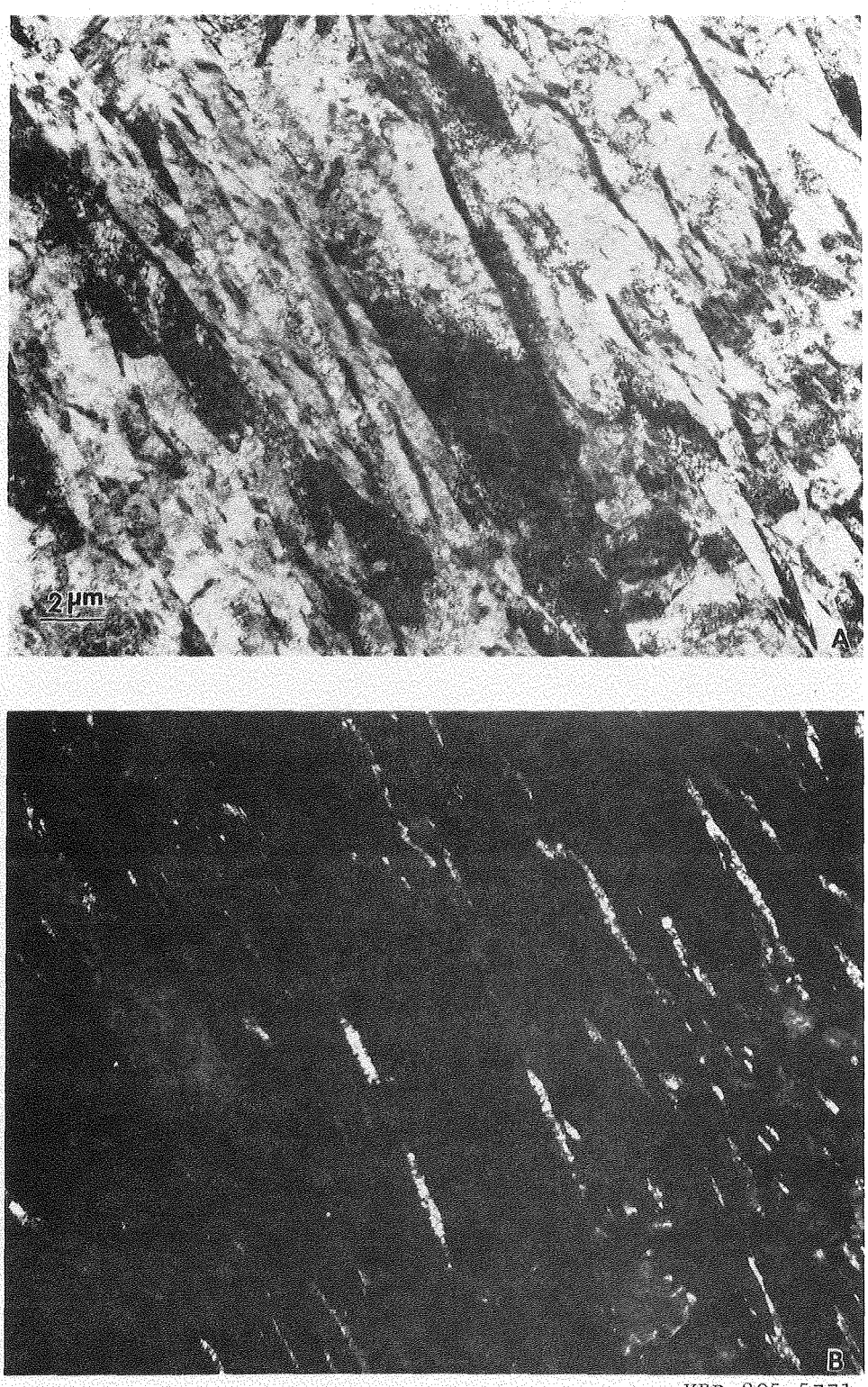

XBB 805 5771

Fig. 13

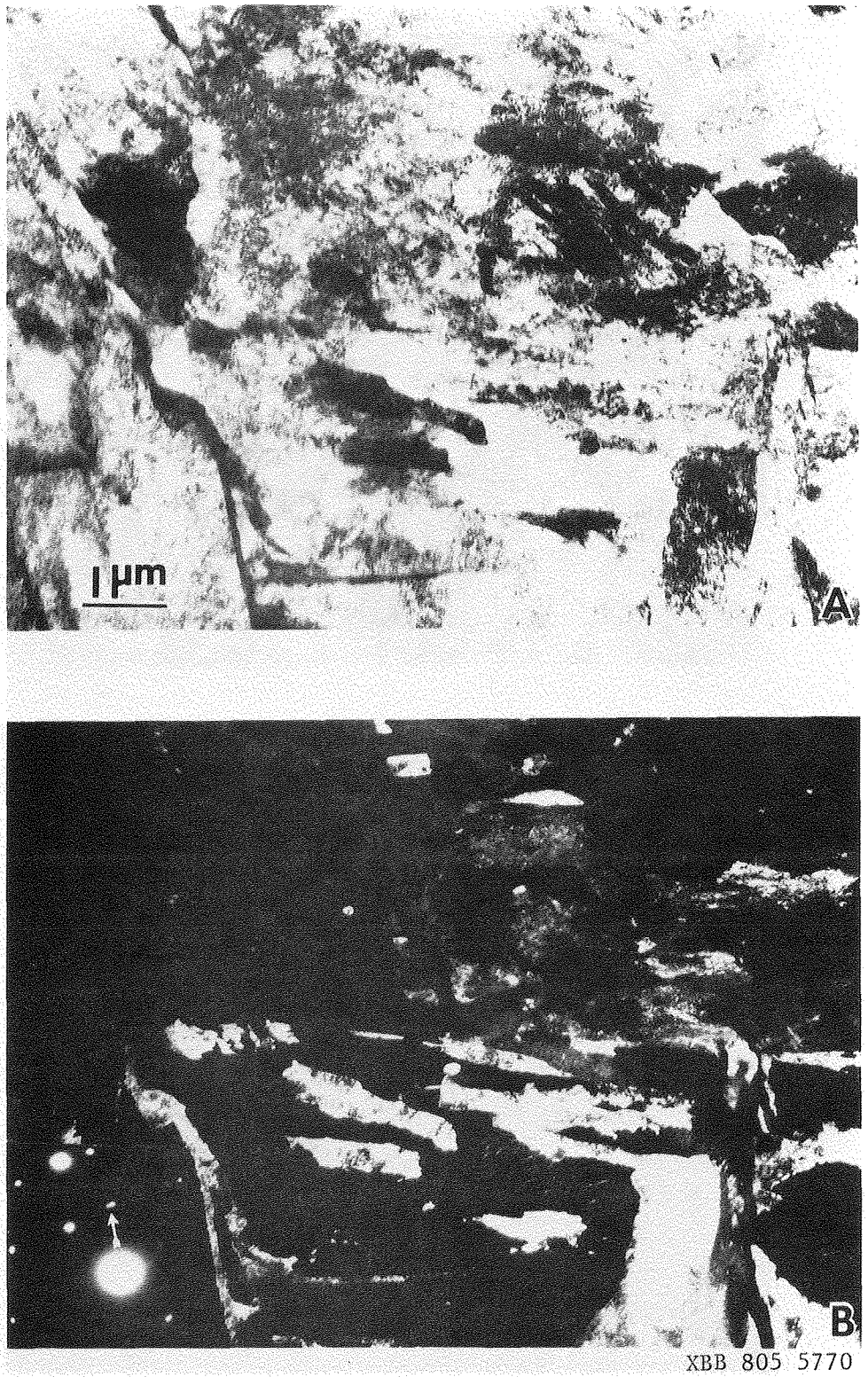

Fig. 14

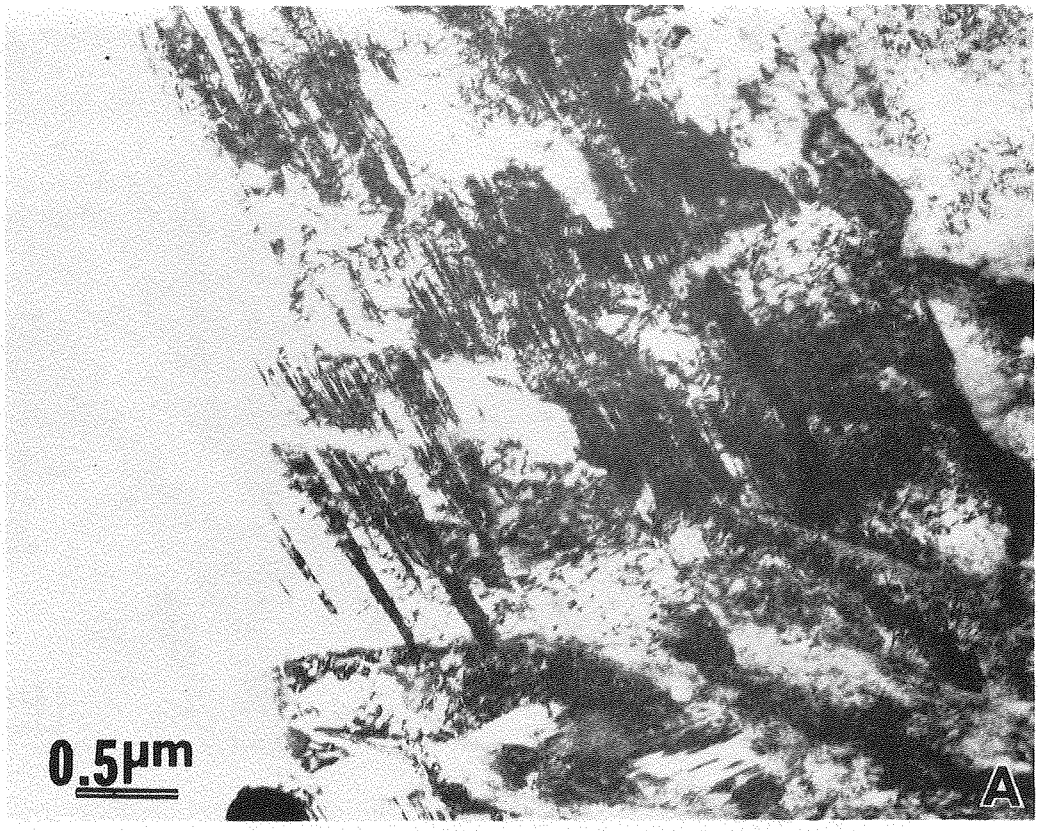

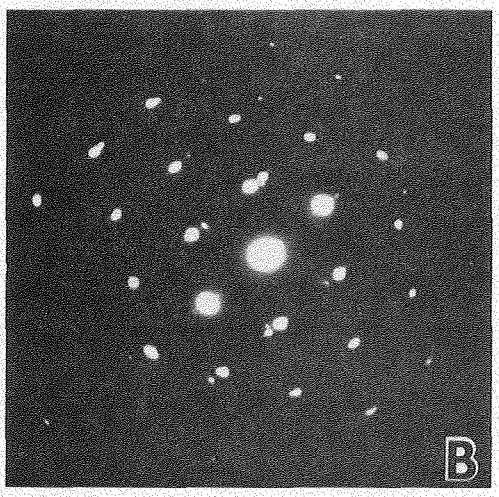

XBB 805 5766

Fig. 15

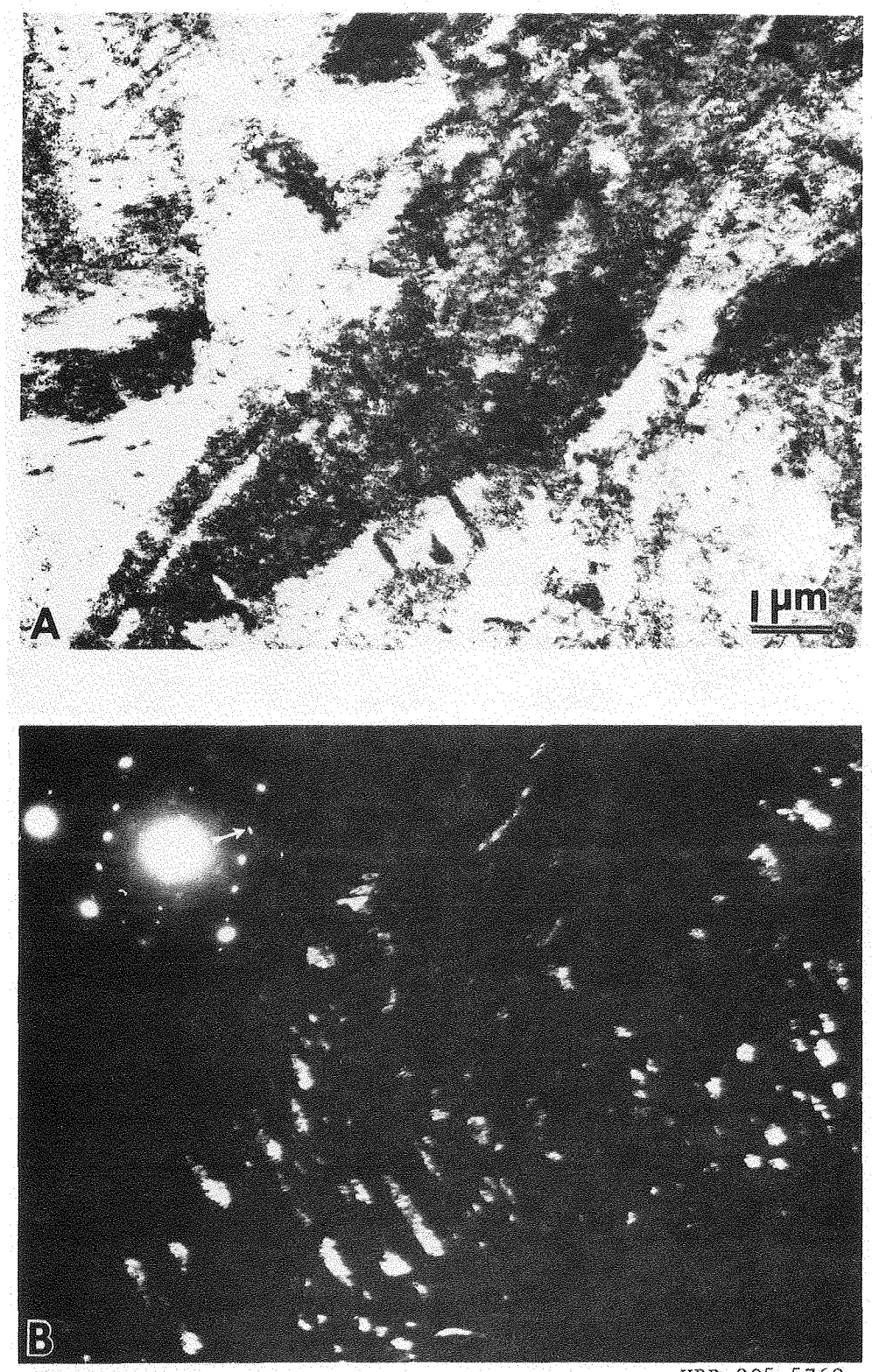

XBB 805 5768

Fig. 16

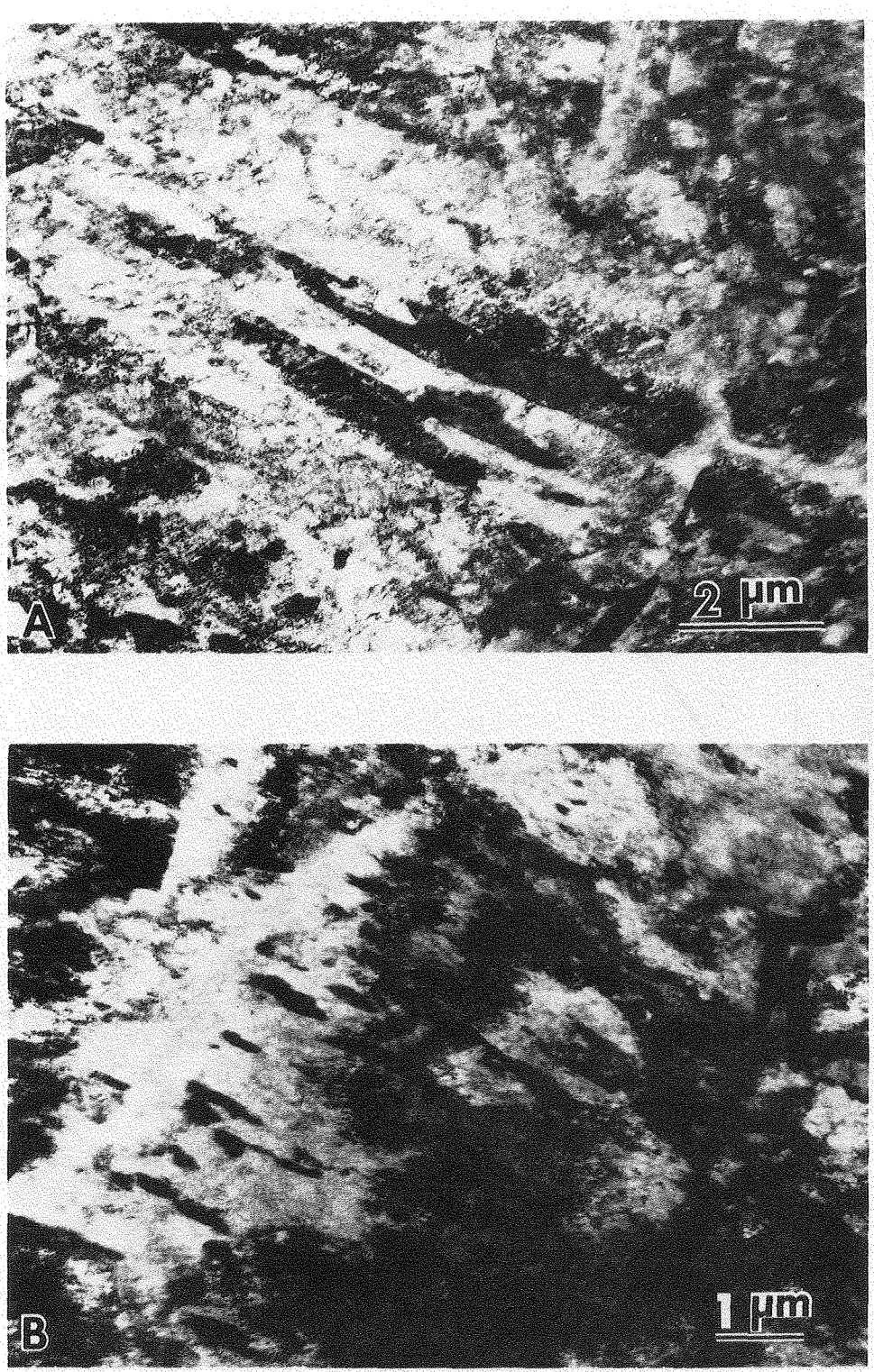

XBB 805 5769

Fig. 17

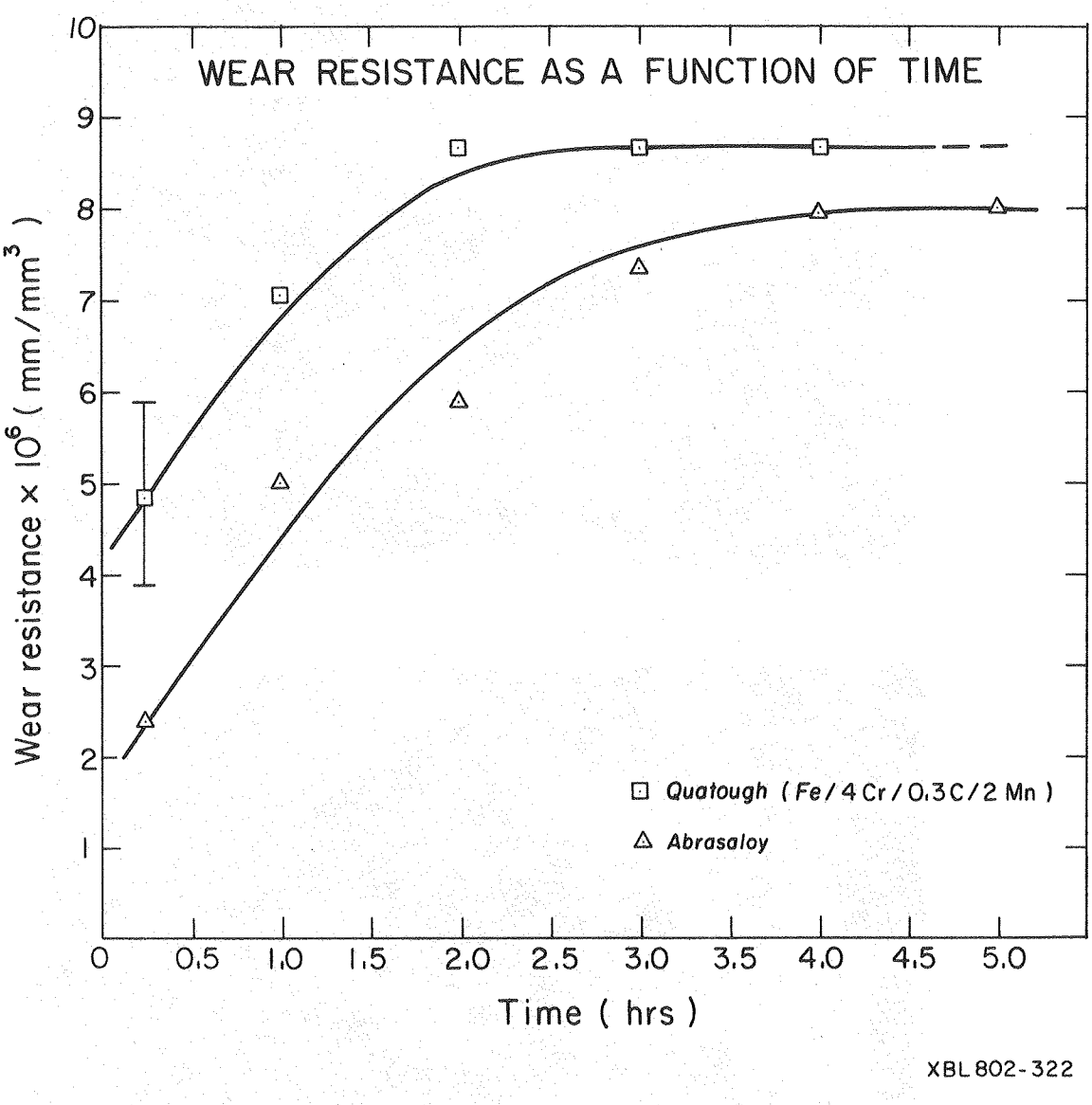
WEAR RESISTANCE AS A FUNCTION OF TIME
Wear resistance x 10^6 (mm/mm^3)
Time (hrs)
Quatough (Fe / 4 Cr / 0.3 C / 2 Mn)
Abrasaloy
XBL 802-322

Fig. 18

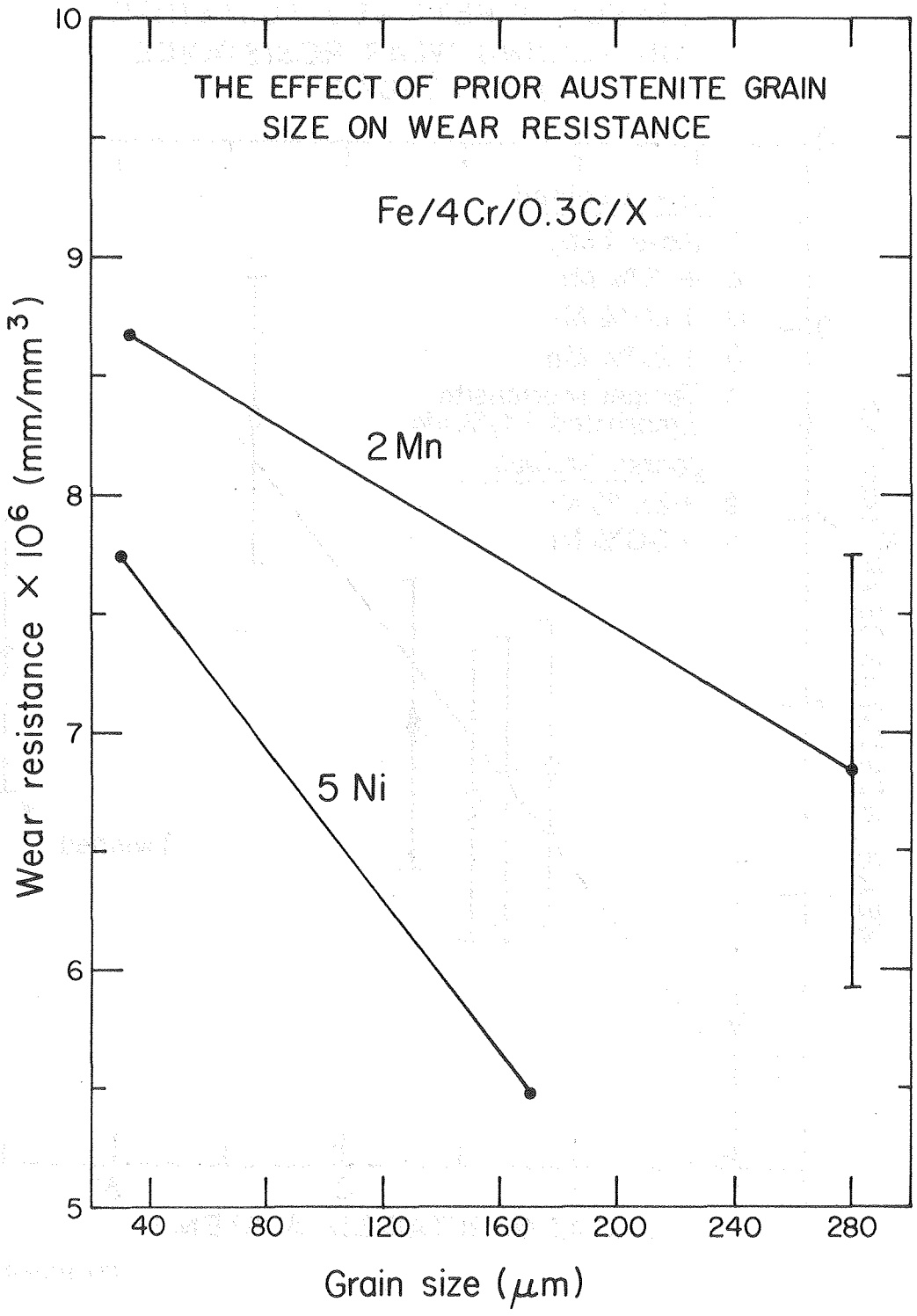

XBL 7911-13212

Fig. 19

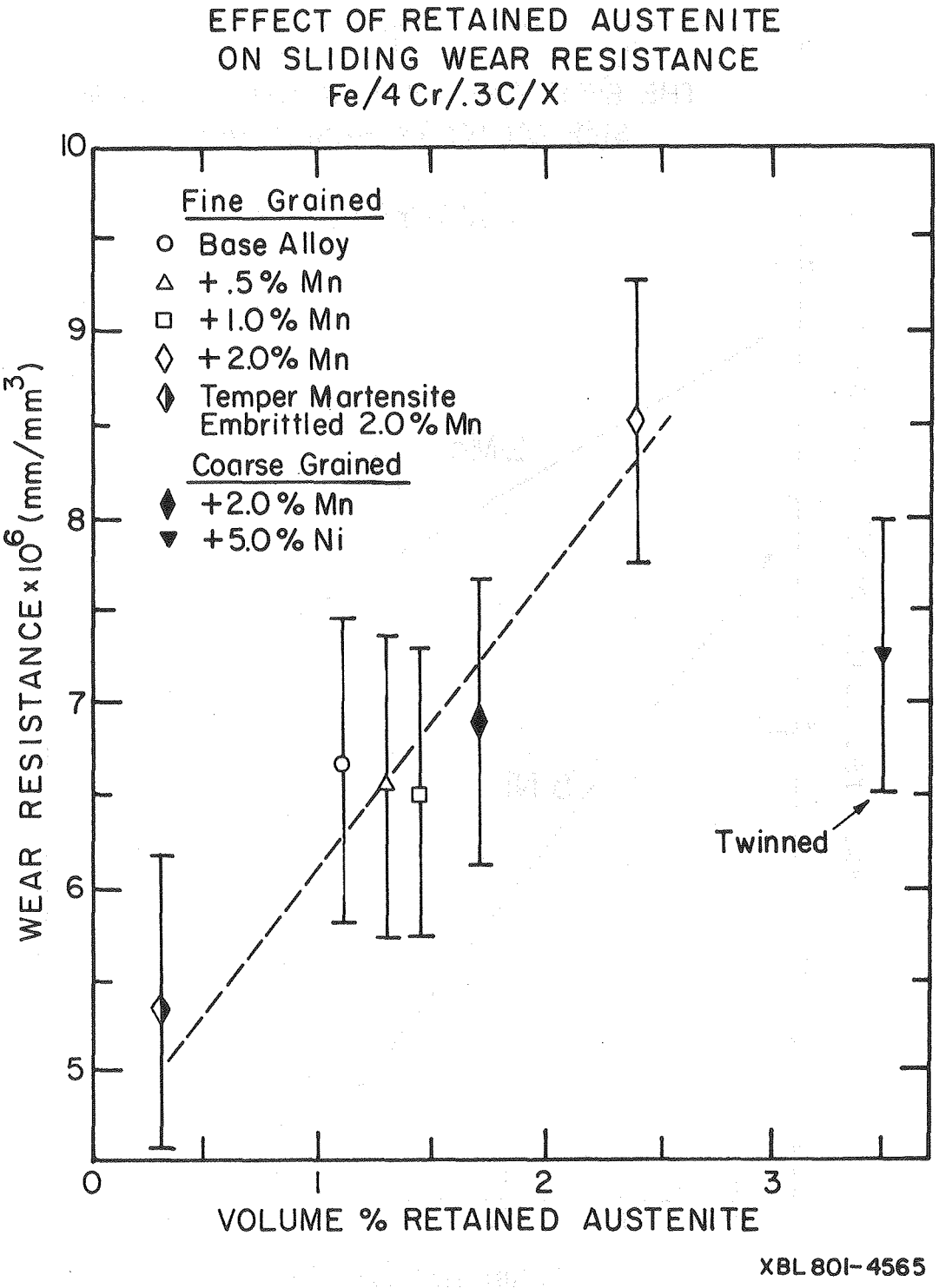
EFFECT OF RETAINED AUSTENITE
ON SLIDING WEAR RESISTANCE
Fe/4 Cr/.3C/X
Fine Grained
Base Alloy
+.5% Mn
+1.0% Mn
+2.0% Mn
Temper Martensite
Embrittled 2.0% Mn
Coarse Grained
+2.0% Mn
+5.0% Ni
Twinned
WEAR RESISTANCE x 10^6 (mm/mm^3)
VOLUME % RETAINED AUSTENITE
0
1
2
3
5
6
7
8
9
10
XBL 801-4565

Fig. 20

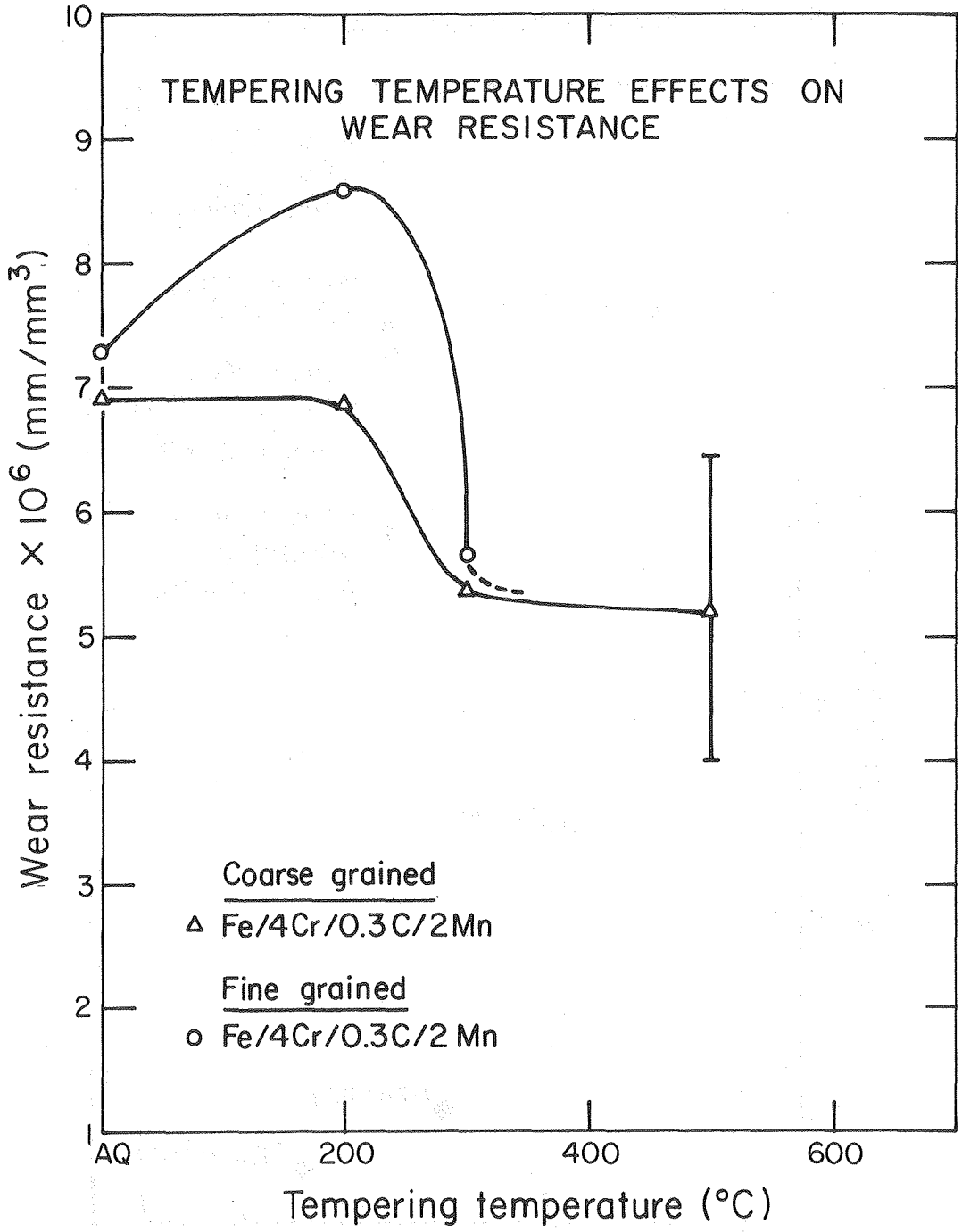
TEMPERING TEMPERATURE EFFECTS ON
WEAR RESISTANCE
Wear resistance × 10⁶ (mm/mm³)
10
9
8
7
6
5
4
3
2
1
AQ
200
400
600
Tempering temperature (°C)
Coarse grained
Δ Fe/4Cr/0.3C/2Mn
Fine grained
o Fe/4Cr/0.3C/2 Mn
XBL 7911-13213

Fig. 21

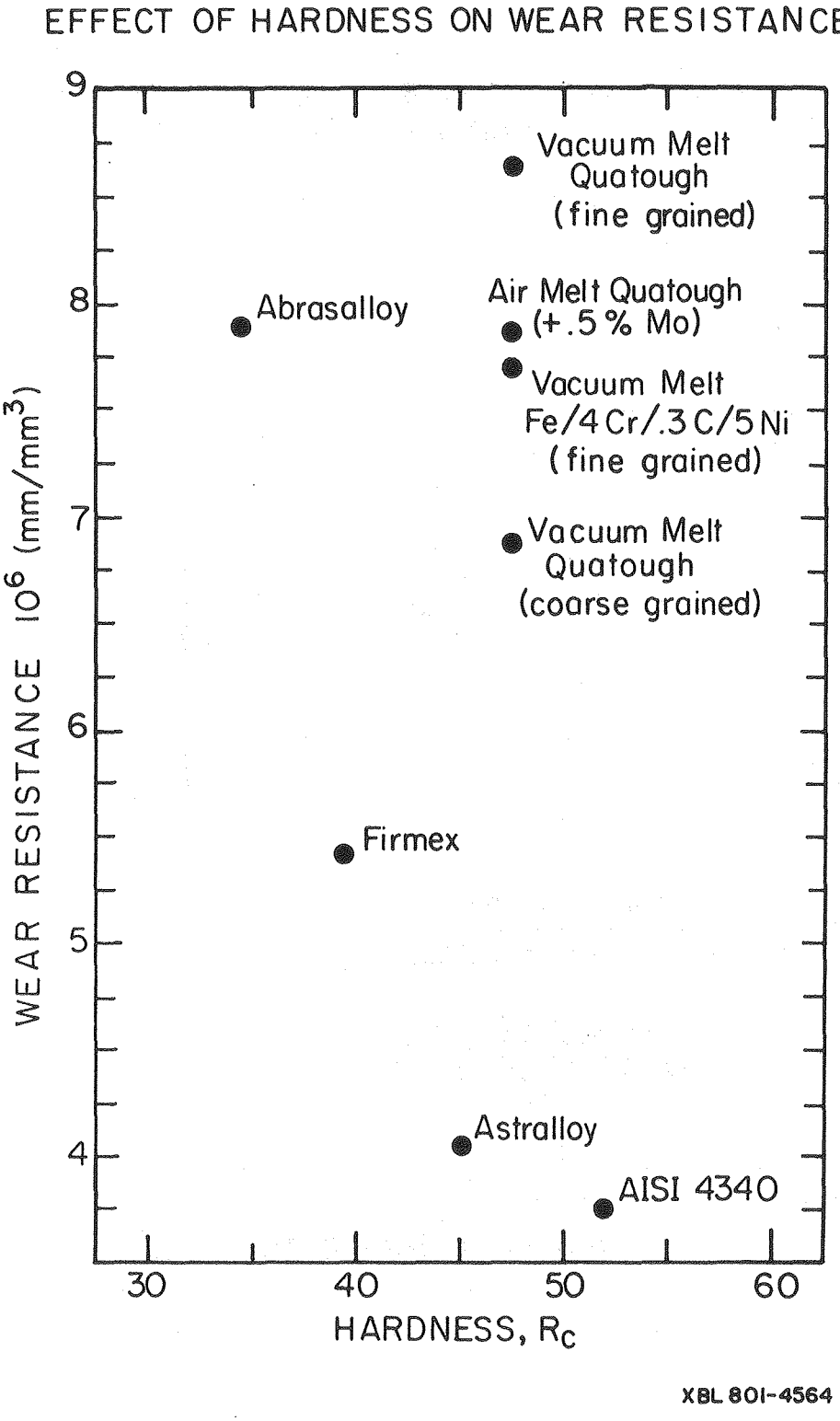
EFFECT OF HARDNESS ON WEAR RESISTANCE
WEAR RESISTANCE 10^6 (mm/mm^3)
9
8
7
6
5
4
Vacuum Melt
Quatough
(fine grained)
Abrasalloy
Air Melt Quatough
(+.5 % Mo)
Vacuum Melt
Fe/4 Cr/.3 C/5 Ni
(fine grained)
Vacuum Melt
Quatough
(coarse grained)
Firmex
Astralloy
AISI 4340
30
40
50
60
HARDNESS, R_C
XBL 801-4564

Fig. 22

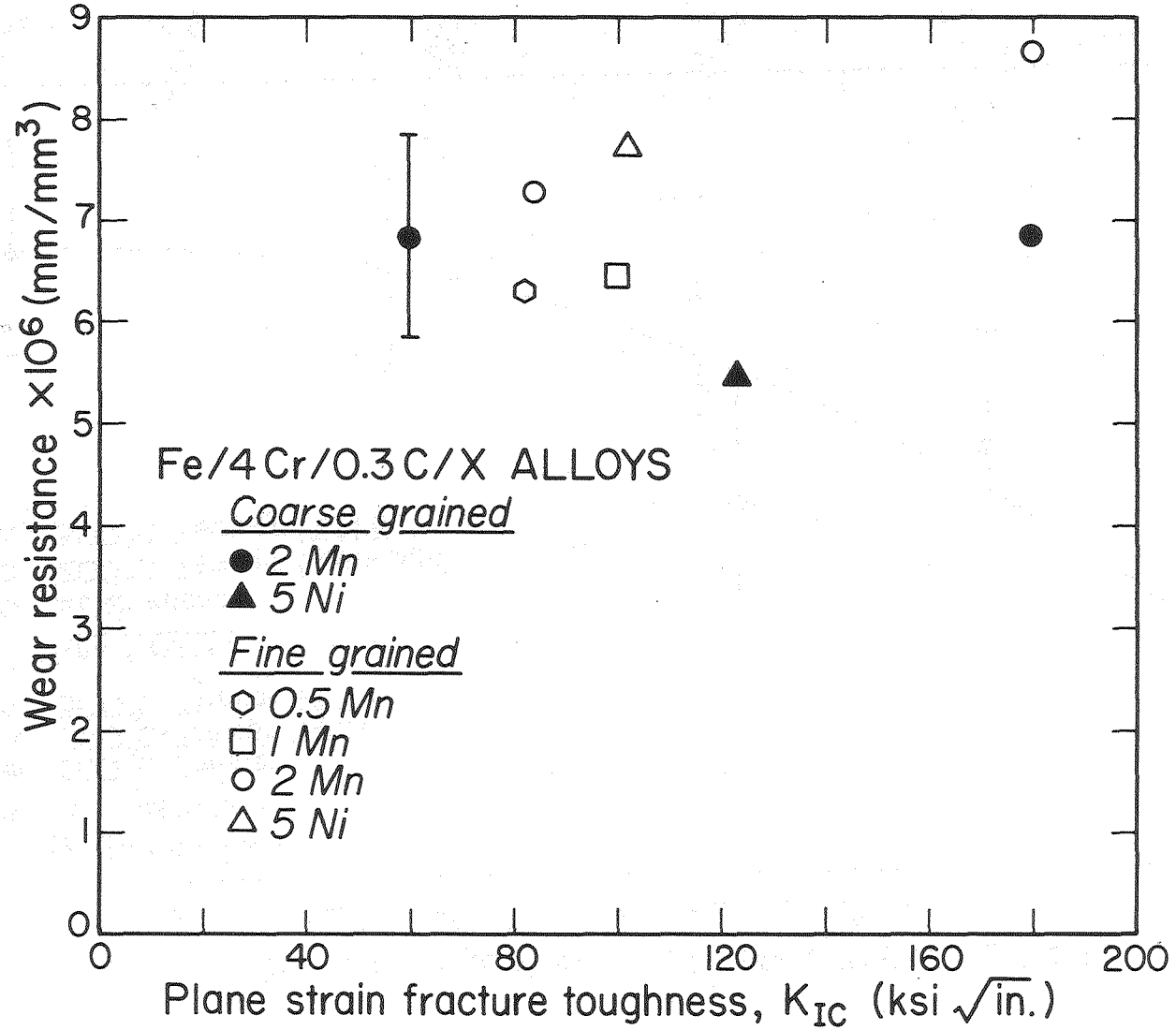

XBL 802-323

Fig. 23

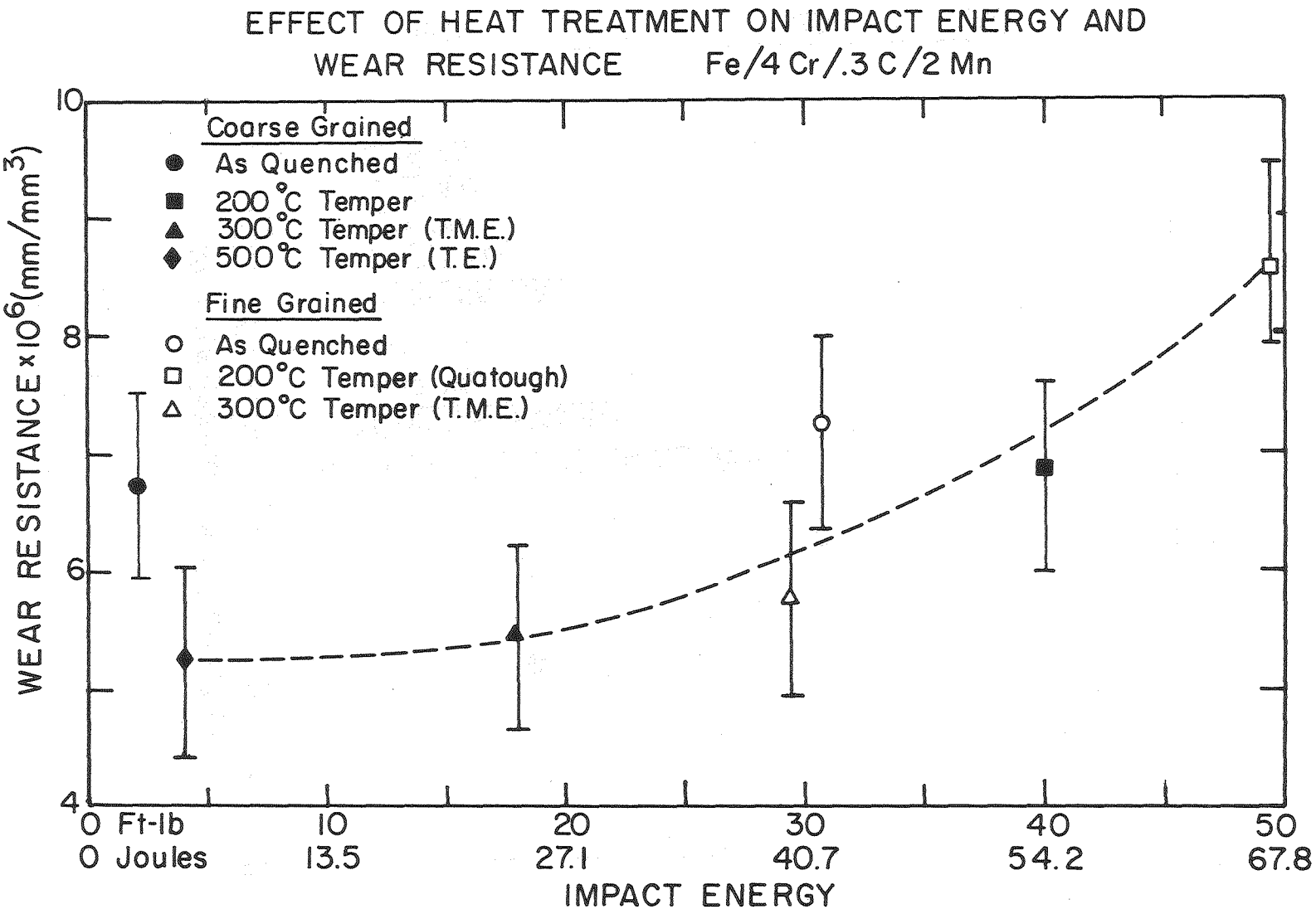
EFFECT OF HEAT TREATMENT ON IMPACT ENERGY AND
WEAR RESISTANCE Fe/4 Cr/.3 C/2 Mn
Coarse Grained
As Quenched
200 °C Temper
300 °C Temper (T.M.E.)
500 °C Temper (T.E.)
Fine Grained
As Quenched
200°C Temper (Quatough)
300°C Temper (T.M.E.)
WEAR RESISTANCE x 10^6 (mm/mm^3)
10
8
6
4
0 Ft-lb
0 Joules
10
13.5
20
27.1
30
40.7
40
54.2
50
67.8
IMPACT ENERGY
XBL 801-4563

Fig. 24

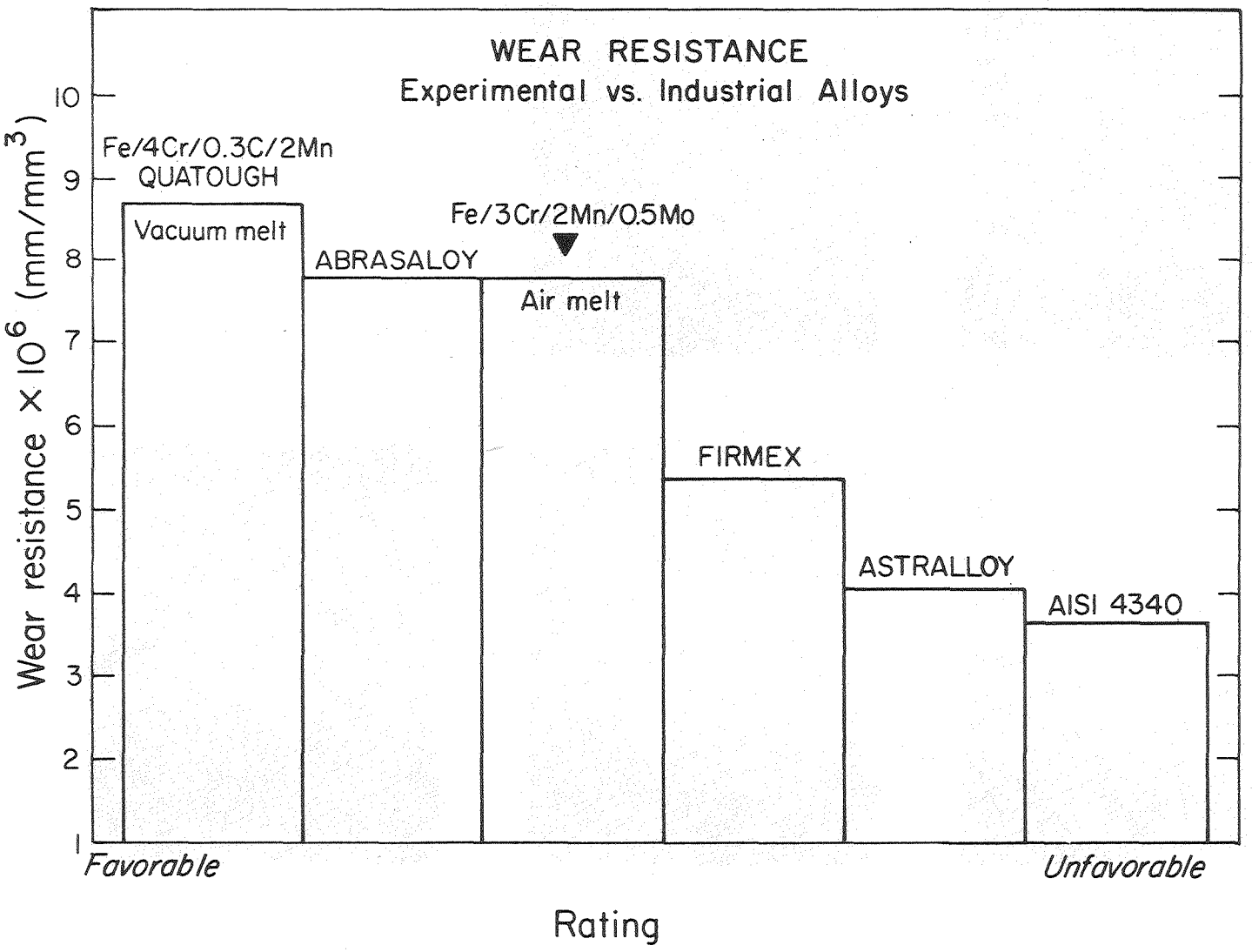
WEAR RESISTANCE
Experimental vs. Industrial Alloys
Wear resistance X 10^6 (mm/mm^3)
10
9
8
7
6
5
4
3
2
1
Fe/4Cr/0.3C/2Mn
QUATOUGH
Vacuum melt
ABRASALOY
Fe/3Cr/2Mn/0.5Mo
Air melt
FIRMEX
ASTRALLOY
AISI 4340
Favorable
Unfavorable
Rating
XBL7911-13211

Fig. 25

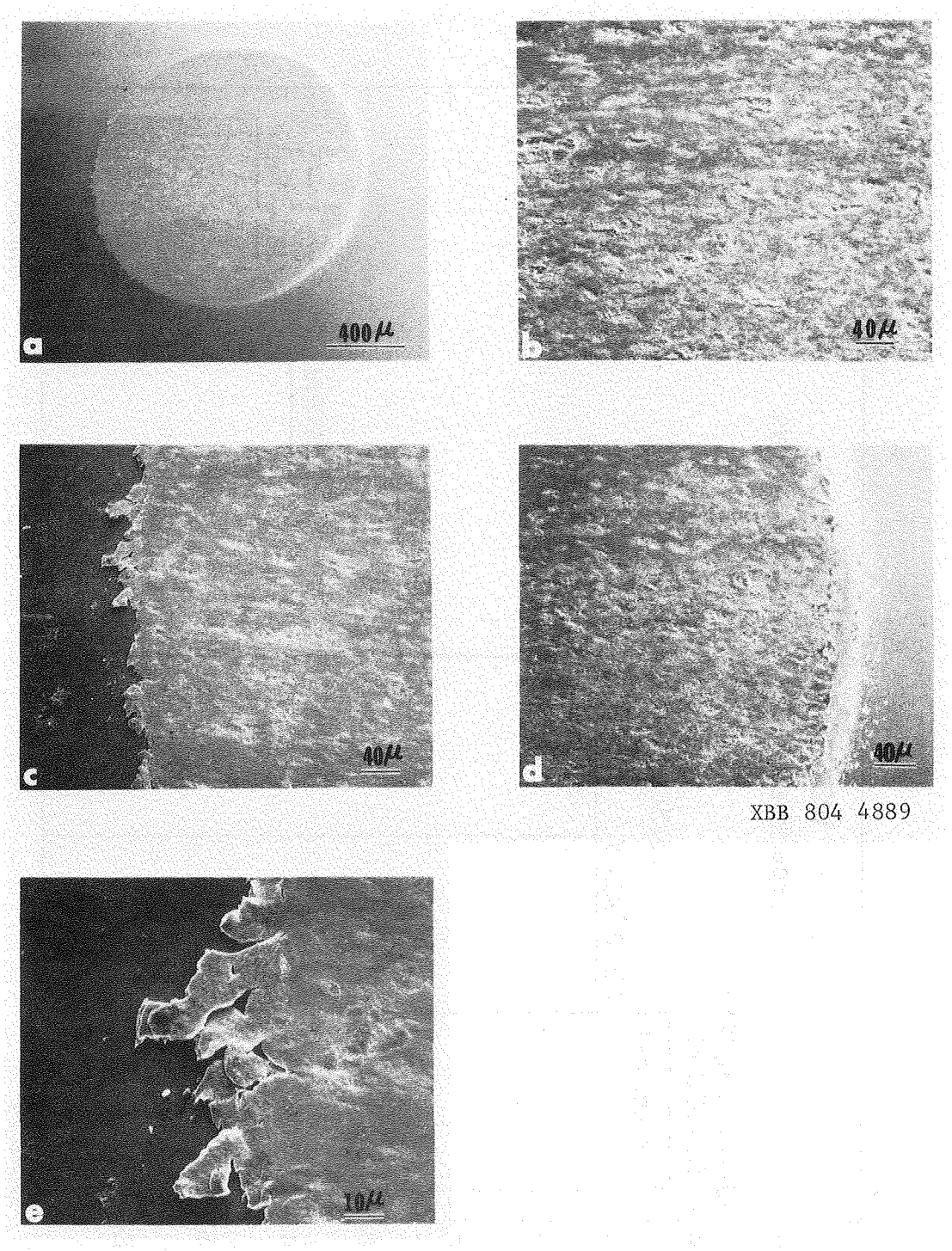

XBB 804 4889

Fig. 26

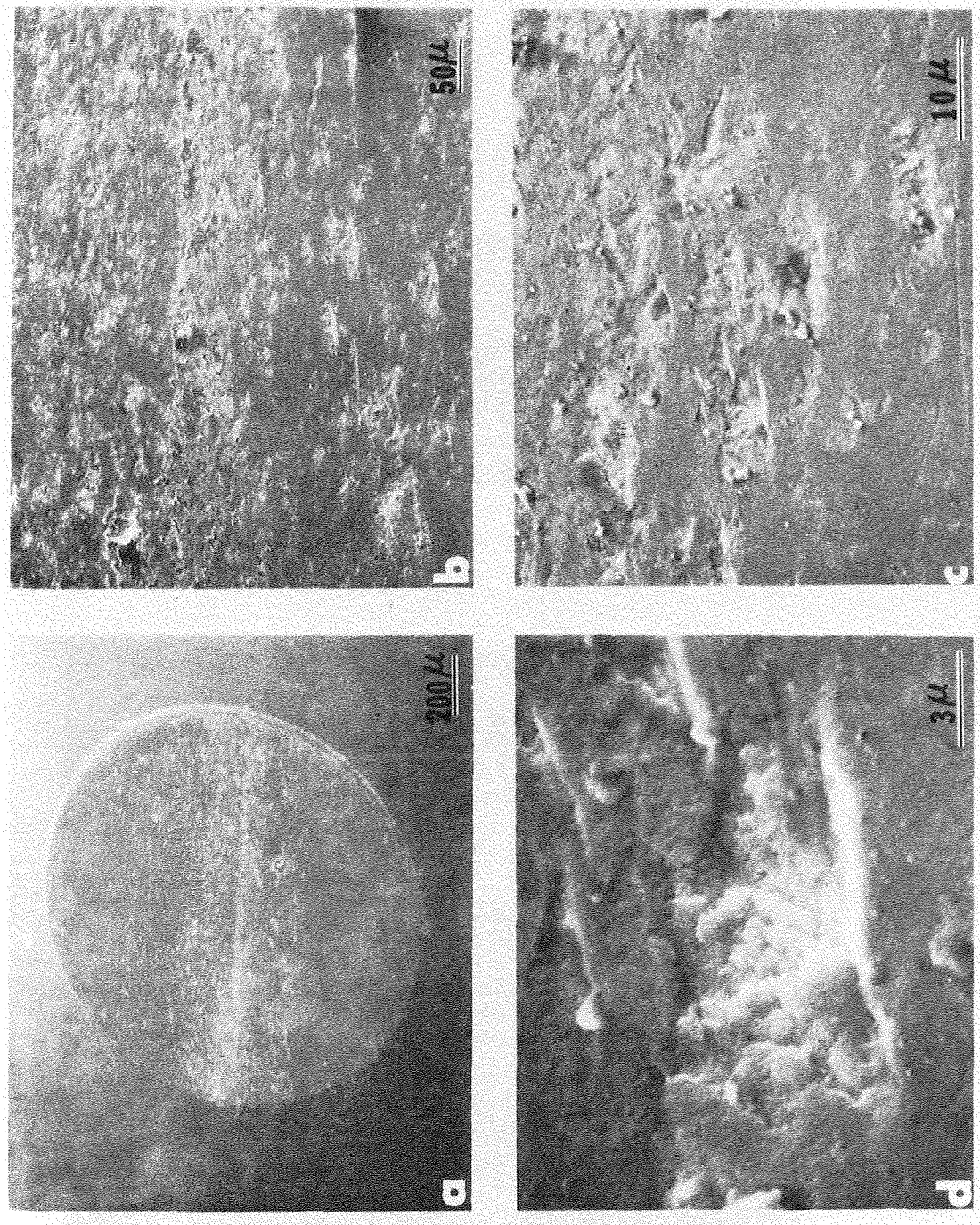

XBB 805 4885

Fig. 27

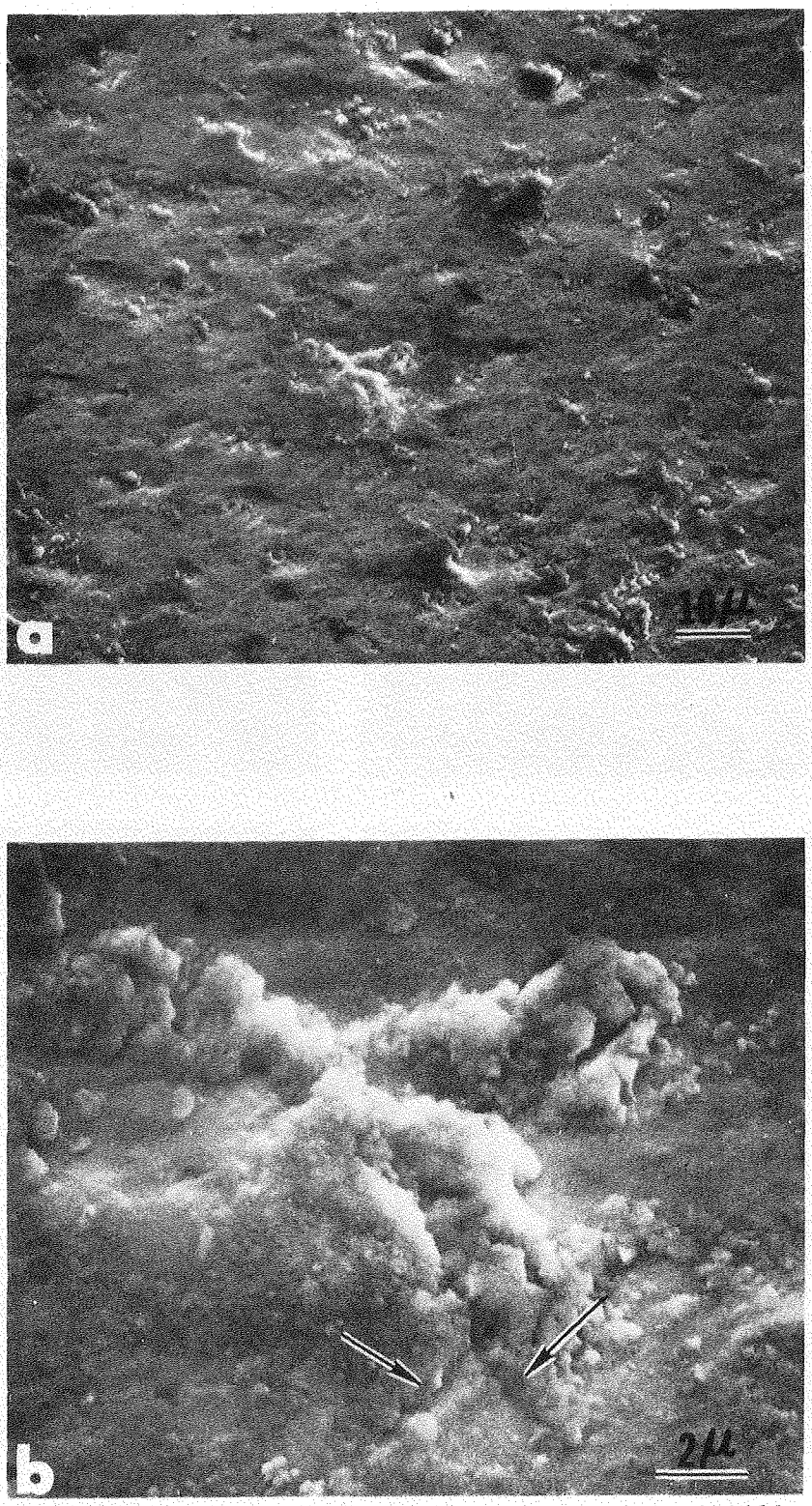

XBB 804 4888

Fig. 28

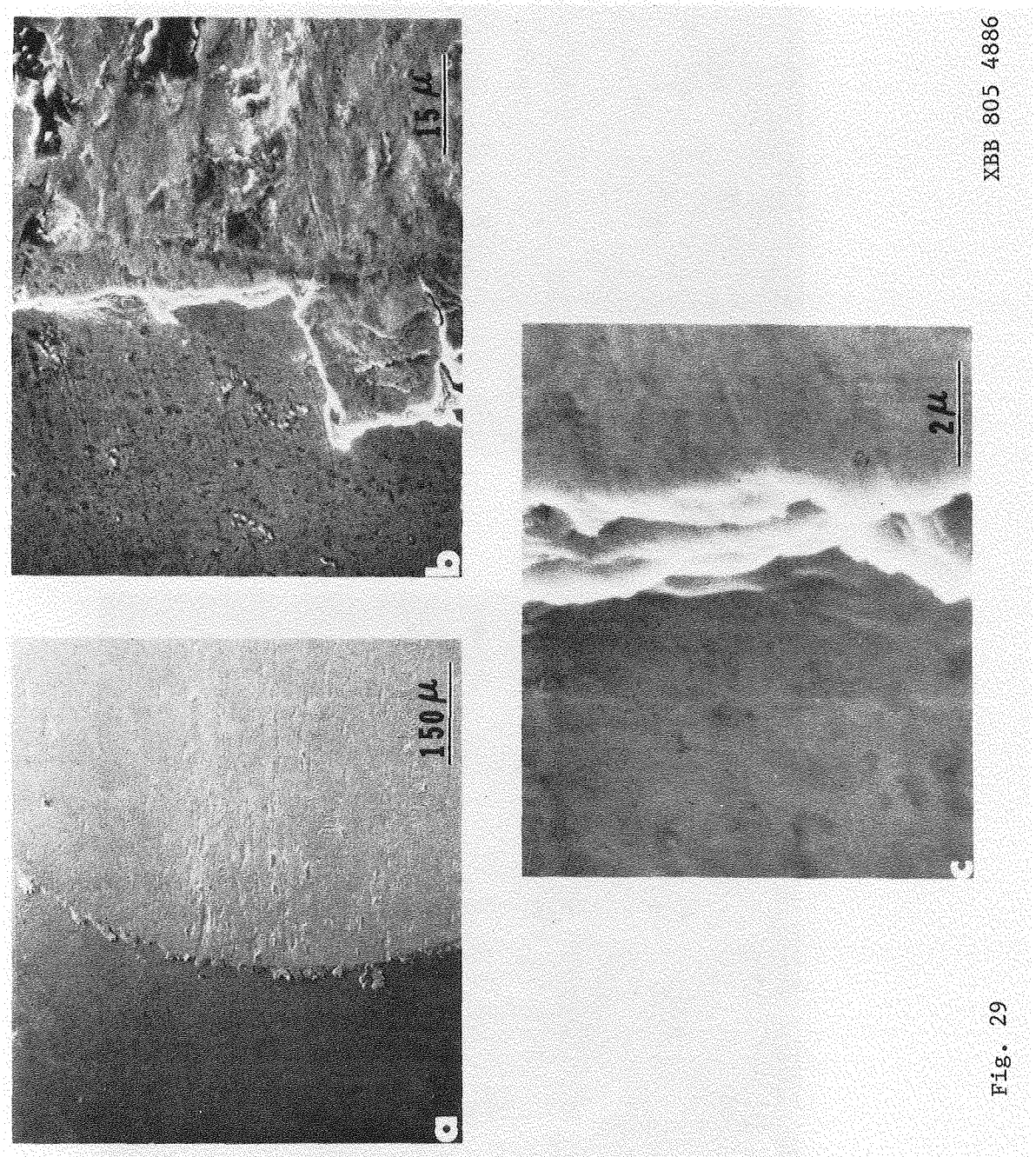

Fig. 29

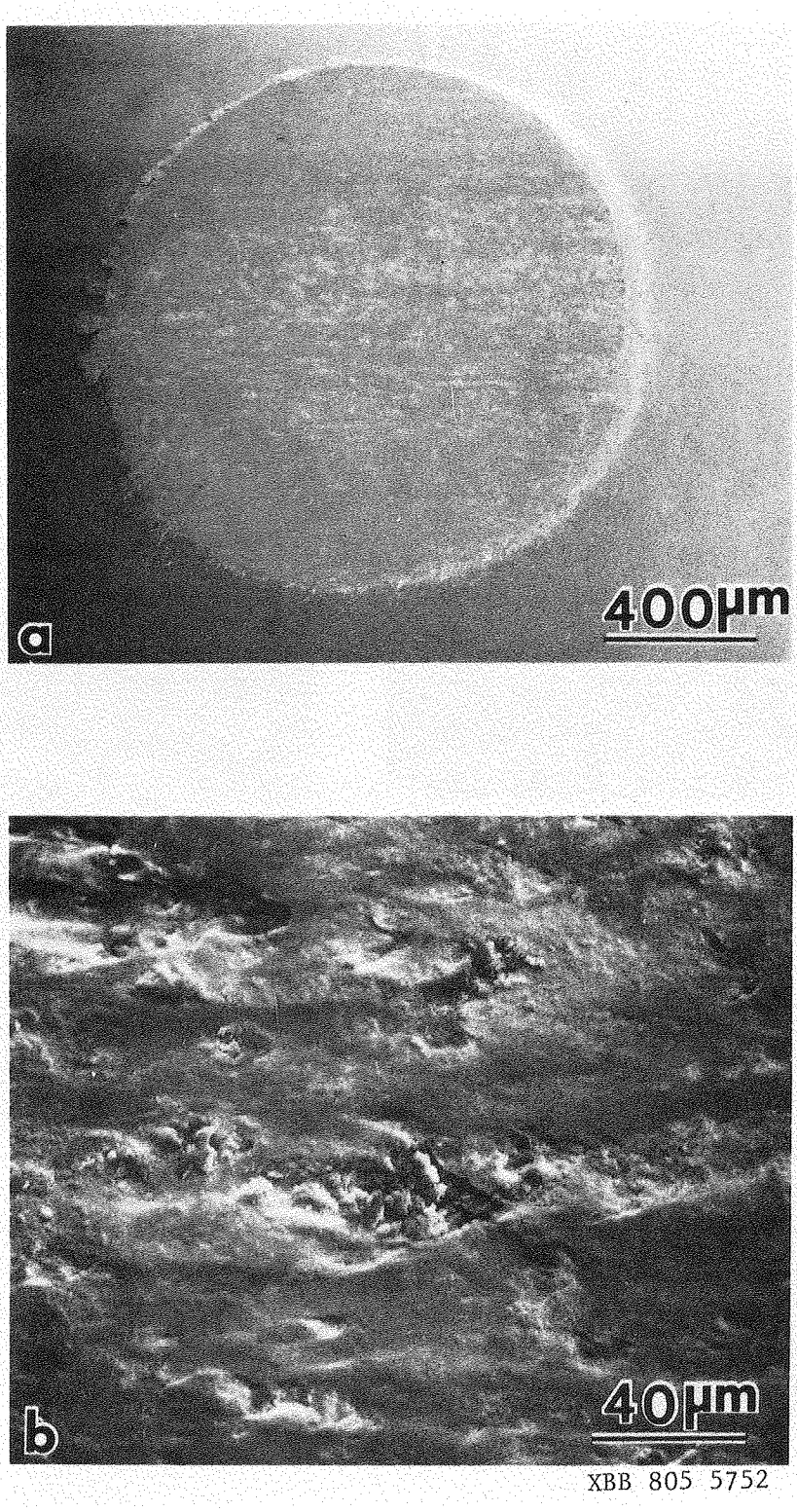

XBB 805 5752

Fig. 30

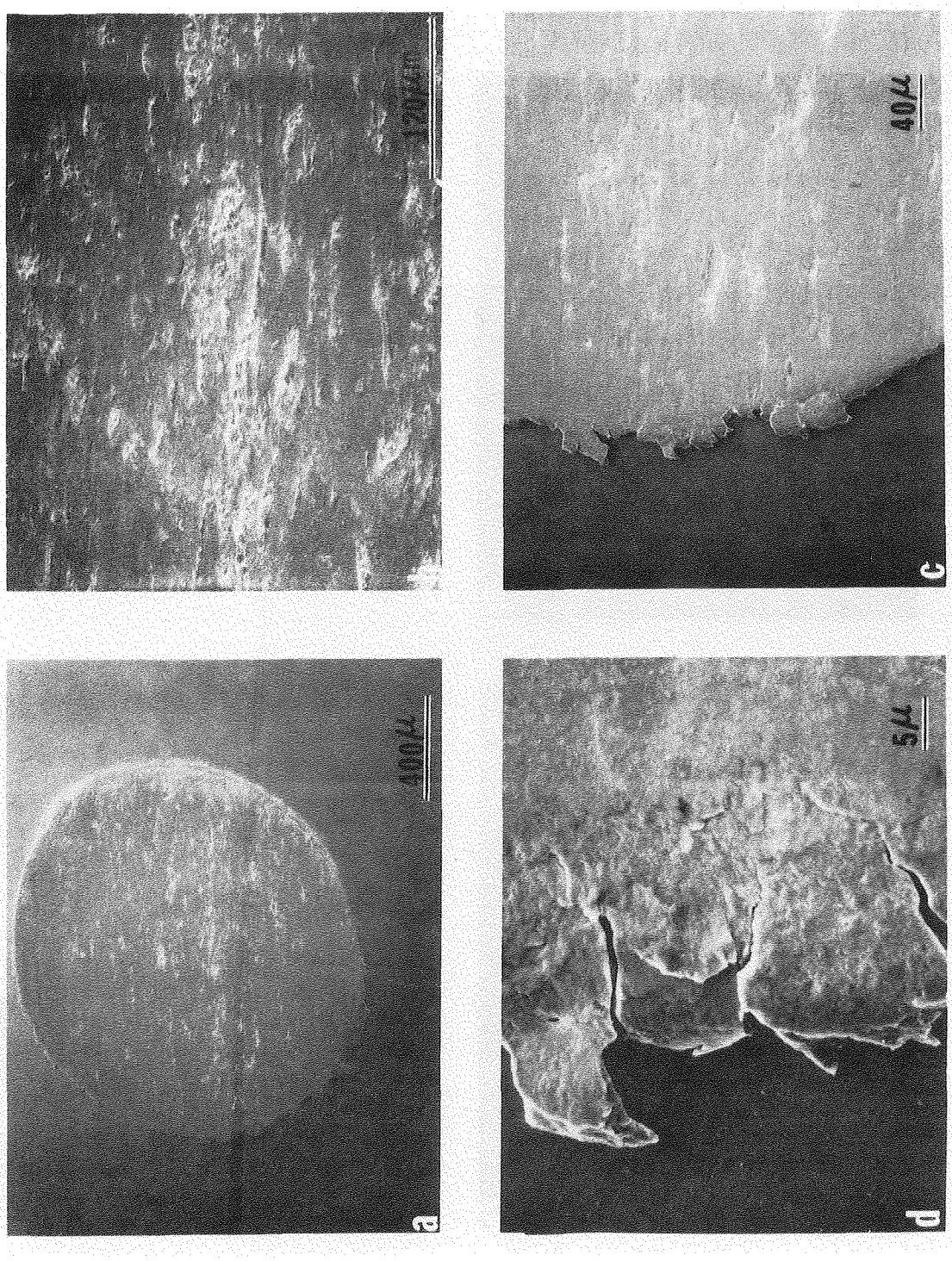

Fig. 31

XBB 805 5753

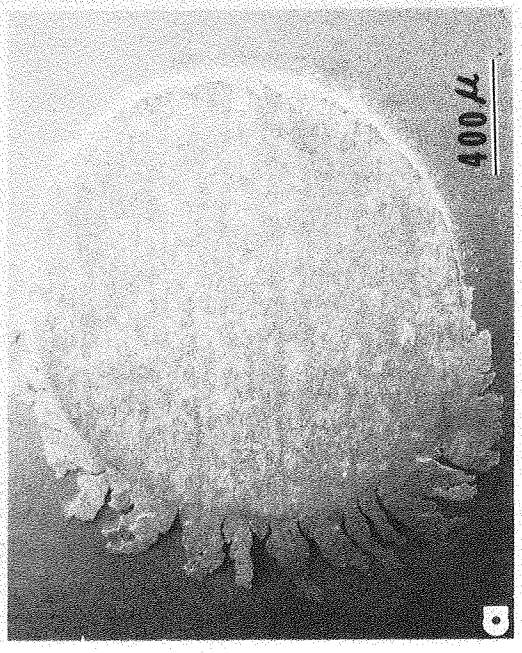

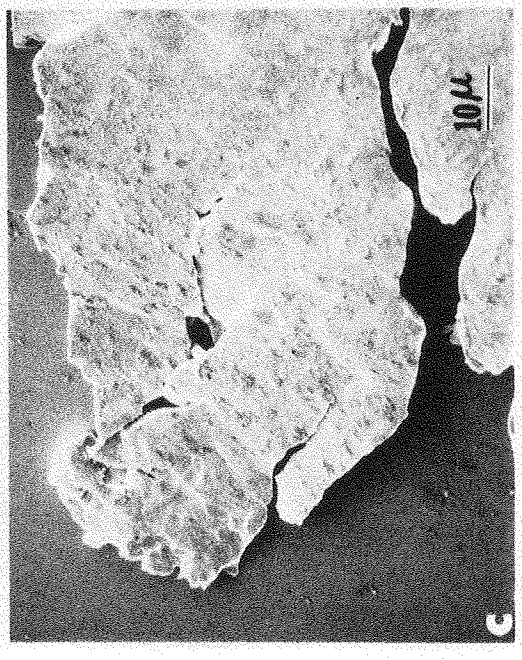

XBB 805 4887

Fig. 32